FGF 18 Augments Bone Healing & Osseointegration of Intra-Medullary Femoral Implants in Osteopenic Bone

Alberto Carli, MD, MSc Candidate

Department of Experimental Surgery

McGill University

Montreal, Québec

Canada

May 2012

A thesis submitted to McGill University, Faculty of Graduate and Postdoctoral Studies, in partial fulfillment of the requirements of the Degree of Masters of Science in Experimental Surgery

TABLE OF CONTENTS

ABSTRACT

Introduction:

Internal fixation of fractures in the presence of osteopenia has been associated with a failure rate as high as 25%. Enhancing bone formation and osseointegration of orthopaedic hardware is a priority when treating patients with impaired bone regenerative capacity. Fibroblast Growth Factor (FGF) 18 regulates skeletal development and could therefore have applications in implant integration. This study was designed to determine if FGF 18 promotes bone formation and osseointegration in the osteopenic $FGFR3^{-/-}$ mouse and to examine its effect on bone marrow derived mesenchymal stem cells (MSCs).

Methods: In Vivo: Intramedullary implants were fabricated from 0.4 x 10mm nylon rods coated with 300nm of titanium by physical vapour deposition. Skeletally mature, age matched female $FGFR3^{-/-}$ and wild type mice received bilateral intramedullary femoral implants. Left femurs received an intramedullary injection of 0.1µg of FGF 18 (courtesy Merck Serono), and right femurs received saline only. Six weeks later, femurs were harvested, radiographed, scanned by micro CT, and processed for undecalcified for histology.

In Vitro: MSCs were harvested from femurs and tibiae of skeletally mature age matched $FGFR3^{-/-}$ and wild type mice. Cells were cultured in Alpha Modified Eagle's Medium (αMEM) to monitor proliferation or αMEM supplemented with ascorbic acid and sodium beta-glycerophosphate to monitor differentiation.

Proliferation was assessed through cell counts and metabolic activity at days 3, 6 and 9. Differentiation was assessed through staining for osteoblasts and mineral deposition at days 6, 9 and 12.

Results: Wild type mice exhibited more peri-implant bone formation compared to $FGFR3^{-/-}$ mice. Peri-implant bone formation at the proximal metaphyseal-diaphyseal junction was increased in FGF18 treated femurs compared with contralateral control femurs in wild type (p = NS) and $FGFR3^{-/-}$ (p = 0.04) mice. Histological analysis corroborated micro CT findings, with FGF 18 treated $FGFR3^{-/-}$ femurs forming peri-implant bone instead of the fibrous response seen in controls. In vitro studies showed that FGF18 significantly increased MSC proliferation and metabolism in a dose dependent manner in wild type and $FGFR3^{-/-}$ mice. Osteoblast differentiation was inhibited by FGF18 in wild type MSCs, while no significant effect was observed in cells harvested from $FGFR3^{-/-}$ mice.

Conclusion: FGF 18 increases bone formation and osseointegration of intramedullary implants in osteopenic mice and increases MSC proliferation in both the presence and absence of FGFR3. FGF18 also inhibits early osteoblast differentiation in the presence of FGFR3. FGF 18 mediated MSC proliferation and osteogenesis is likely due to signalling through an alternate FGFR, likely FGFR1 or 2. Additional work is needed to confirm the identity of the alternate FGFR and to evaluate its capacity to improve osseous healing in unfavourable in-vivo environments.

RÉSUMÉ

Introduction: La fixation interne de fractures dans la présence de l'ostéopénie a été associée à un taux d'échec aussi élevé que 25%. Amélioration de la formation osseuse et l'ostéo-intégration de matériel orthopédique est une priorité pour le traitement de patients. Facteur de croissance des fibroblastes (FGF) 18 régit le développement squelettique et pourrait donc avoir des applications dans intégration de l'implant. Cette étude a été conçue pour déterminer si le FGF 18 favorise la formation osseuse et l'ostéo-intégration dans le ostéopénique FGFR3$^{-/-}$ souris et d'examiner son effet sur la moelle osseuse provenant de cellules souches mésenchymateuses (CSM).

Méthodes: Implants intramédullaires ont été fabriqués à partir de tiges de nylon 10mm x 0,4 revêtus de 300nm de titane par dépôt de vapeur physique. Les souris de type FGFR3$^{-/-}$ et souris de type sauvage a reçu des implants intramédullaires au femurs. Les fémurs gauche ont reçu une injection intra-médullaire de 0.1µg de FGF 18 (Merck Serono), et les fémurs droit ont reçu une solution saline seule. Après six semaines, les fémurs ont été récoltés, analysé par les micro CT, et préparé pour l'histologie. Les CSM ont été récoltées à partir de fémurs et les tibias de souris de type FGFR3-/ - et de type sauvage. Les cellules ont été cultivées dans ‘Alpha Modified Eagle’s Medium’ (aMEM) pour surveiller la proliferation, ou cultivées dans un milieu ‘aMEM’ complété avec de l'acide ascorbique et de sodium bêta-glycérophosphate pour surveiller la différenciation. La prolifération a été évaluée par dénombrement des cellules et l'activité métabolique aux jours 3, 6 et 9. Différenciation a été évaluée par

coloration pour les ostéoblastes et les dépôts minéraux aux jours 6, 9 et 12.

Résultats: Les souris de type sauvage ont produit plus d'os péri-implantaire par rapport à FGFR3-/ - souris. La formation osseuse péri-implantaire à la jonction proximale métaphysodiaphysaire a été augmenté en fémurs traités avec FGF18 par rapport aux fémurs de contrôle controlatéraux dans de type sauvage ($p > 0.05$) et FGFR3-/ - ($p = 0.04$). L'analyse histologique a corroboré les conclusions micro CT. Les femurs FGFR3-/ - qui ont recus FGF 18 traités fémurs ont formé l'os autour de l'implant au lieu de la réponse fibreuse vu dans les contrôles. Des études in vitro ont montré que la proliferation du MSC ont été augmenté avec FGF18 d'une manière dose-dépendante pour les type sauvage et les type FGFR3-/ -. La différenciation des ostéoblastes a été inhibée par FGF18 pour les CSM du type sauvage. Aucun effet significatif sur la différenciation a été observé dans les cellules récoltées à partir de souris FGFR3-/ -.

Conclusion: FGF 18 augmente la formation osseuse et l'ostéo-intégration des implants intramédullaires chez la souris ostéopéniques. FGF 18 augmente la prolifération des CSM à la présence et l'absence de FGFR3. FGF18 inhibe également la différenciation ostéoblastique a la présence de FGFR3. Les effets de FGF 18 sur le prolifération des CSM et l'ostéogenèse est probablement dû à la signalisation grâce à un FGFR alternative, probablement FGFR1 ou 2. Des travaux in vivo supplémentaires sont nécessaires pour confirmer l'identité de l'autre FGFR et d'évaluer sa capacité à améliorer la cicatrisation de l'os en environnements défavorable.

CONTRIBUTIONS OF AUTHORS

Alberto Carli: Methodology planning, performed surgical procedures, harvested specimens, micro CT scans, cell experiment analysis, statistical analysis, manuscript preparation and editing.

Chan Gao: Taught surgical procedures, micro CT scans, contributed to data analysis, manuscript editing

Maedeh Khayyat-Kholghi: Assisted in cell experiment methodology planning, in vitro data collection and analysis

Ailian Li: Taught histological techniques, prepared histological data

Huifen Wang: Taught in vitro techniques and animal care, assisted in data collection.

Christoph Ladel: Methodology planning, statistical analysis and manuscript editing

Janet E Henderson: Methodology planning, overall data analysis, manuscript preparation and editing

Edward J Harvey: Methodology planning, overall data analysis, manuscript preparation and editing

ACKNOWLDEGEMENTS

I would like to express my sincerest gratitude to Drs. Edward Harvey and Janet Henderson, whose expertise and mentorship have assisted me in making the most out of my graduate experience and encouraged me to continue on my path toward becoming a surgeon scientist.

I am also indebted to the teaching and collegiality that was offered to me by C Gao, H Wang, A Li, M Khayat Kholghi, M Sullivan and C Ladel. This work would not have been possible without their proficiency and time.

I would like to thank Kelly Stelmaszczyk for her unwavering love, support and patience throughout this journey. Thank you to my father, who inspired me to be a physician; to my mother, who inspired me to be my best; and to my sister, who reminds me to stay grounded.

LIST OF FIGURES

Please note:
Figures 2-6 were adapted with permission from the following manuscript:
A. Carli, C. Gao, M. Khayyat-Kholgi, A. Li, H. Wang, C. Ladel, E.J. Harvey, J.E. Henderson. FGF 18 Augments Bone Healing and Osseointegration of Intra-Medullary Implants in Osteopenic $FGFR3^{-/-}$ Mice.

1.0 INTRODUCTION

1.1 – Definition and Clinical Impact of Poor Bone Quality

Although lacking a formal definition, bone quality can be described as the product of multiple factors that determine how well the skeleton can resist tensile and compressive forces without fracture[1]. Such factors include the density of osteocytes and calcium hydroxyapatite, the pattern and connectivity of the collagen microarchitecture, the extent of microdamage and the capability for both turnover and repair. These factors are largely interdependent, so that an abnormality in one often leads to changes in others. 'Poor bone quality' therefore refers to any primary abnormality of bone that leads to a greater disposition to fracture. Given that bone densitometry, the traditional measurement of bone strength, has recently been found to not always reliably predict fracture risk[2], interest in further quantifying poor bone quality with animal models has recently emerged. Before such models and resulting therapies can be discussed, it is first necessary to examine the impact disease of poor bone quality have upon society and medical care. This impact is perhaps best represented by the most pervasive disease of poor bone quality, osteoporosis.

Osteoporosis is a disease of poor quality bone which involves the reduction of bone mass, bone strength, and the presence of microarchitectural disruptions that render bone susceptible to fracture from minimal force[3]. Osteoporosis clinically defined by the World Health Organization as a bone mineral density that is 2.5 or more standard deviations below the young adult reference mean as measured by dual-energy x-ray absorptiometry. Osteoporosis

has been categorized into two major types according to underlying cause. Primary osteoporosis includes postmenopausal osteoporosis (type 1), age related or “senile” osteoporosis (type 2), and idiopathic osteoporosis[4]. Secondary osteoporosis encompasses a broad group of inherited or acquired diseases, medications and lifestyles (table 1) that are associated with a reduction in bone quality[5]. Histologically, postmenopausal osteoporosis is marked by thinned, poorly connected bony trabeculae, while senile osteoporosis additionally includes widening of spaces between haversian systems and thinning of normally rigid cortical bone[6].

Osteoporosis is a growing global health problem, currently placing over 100 million people worldwide at risk for developing an osteoporotic fracture[7]. Women figure prominently in this statistic, with two out of five expected to sustain a fragility fracture at some point in their lives after the age of fifty[8]. Since the majority of bone mineral loss in osteoporosis involves cancellous bone[9], the metaphyseal portion of bone (the broader portion of bone that connects the epiphysis and articular surface to the tubular shaped diaphysis) is at a higher risk for sustaining a fracture[10]. Fractures in the metaphyseal regions femoral neck and distal radius, as well as fractures in the anterior half of the vertebral body are classically considered to be osteoporotic fractures. Of these locations, hip fractures are the most prevalent in individuals over 75, at a current rate of 630 to 1289 per 100,000 people[11]. Based on current demographic trends and prolongations in life expectancy, the prevalence of age related osteoporosis is expected to increase by 89% in men and 69% in women over the next fifteen

years. Using this projection, the annual occurrence of osteoporotic hip fractures (which represent only 14% of all osteoporotic fractures) is estimated to be 2.6 million, or over 70,000 per day, by 2025[12]. This statistic is alarming not only due to its economic burden, projected to be $16 billion per year in the United States alone[13], but also due to the finding that the occurrence of any major osteoporotic fracture elevates the risk of death within 5 years of sustaining the fracture by 13-fold[14]. Despite its prevalence and medical burden, osteoporosis continues to both under-diagnosed and undertreated[15].

1.2– Principles of Management of Osteoporotic Fractures

The goal of definitive treatment of fractures in individuals with osteopenic bone includes careful evaluation and treatment of their medical comorbidities and restoration of function as early as possible[16]. Such restoration can be provided through both operative and non-operative means. Non-operative treatment traditionally involves closed reduction of the injured extremity with external immobilization spanning across the fracture site to the joint above and below. External immobilization may consist of a circumferential plaster-of-paris cast, or removable brace/splint. This form of treatment is most commonly performed for extra-articular osteoporotic fractures of the wrist, and is also applicable for specific fracture patterns involving the proximal humerus, clavicle, ankle, and foot. Non-operative treatment is also mandated for any patient who is not fit for surgery due to other medical comorbidities.

Operative treatment of osteoporotic fractures is mandated when conservative management is insufficient in providing a result which is clinically acceptable to the treating physician and/or functionally acceptable to the patient. The AO/ASIF (Arbeitsgemeinschaft für Osteosynthesefragen/ Association for the Study of Internal Fixation) Foundation, a leading global authority for orthopaedic fracture management, has formulated four treatment guidelines for operative fracture treatment[17]:1) anatomical reduction of the fracture fragments; 2) stable internal fixation of fractures to tolerate local biomechanical demands; 3) preservation of soft tissue and blood supply to the injured area of the extremity; and 4) provide treatment to permit active, pain-free mobilization of adjacent muscles and joints. Such guidelines figure prominently in the surgical management of osteoporotic fractures, with stable internal fixation usually being achieved with a variety of orthopaedic implants including wires, screws, plates, and intramedullary nails. Central to the process of internal fixation is the process of 'osseointegration', which can be defined as the formation of a direct interface between bone and implant without the presence of interposed soft tissue. The formation of a direct interface facilitates load transfer from bone to hardware, allowing the patient to weight bear and sparing the fragile fracture site from excessive tension and compression that could impair healing.

1.3 – Limitations of Operative Treatment & Current Hypotheses

Despite techniques to promote fracture union, operative treatment of osteoporotic fractures has been associated with a 50% failure rate[18], a 40% risk

of residual angular deformity and a 23% need for a second operation[19]. The primary mode of failure in operatively treated osteoporotic fractures is bony failure, not implant failure. The cause for bony failure is believed to be multifactorial. Firstly, with thinner cortical and cancellous bone, screw threads have less bony contact, reducing their ability to resist torsional stress and reducing the force needed to pull them out[20,21]. Furthermore, due to the brittle nature of osteoporotic bone, inserting screws or other transcortical implants causes micro and macrofractures which lead to construct instability and possible implant malposition[22]. In addition, the load transmitted at the bone-implant interface, which normally functions to shield the fracture site in order to permit healing, can often exceed the tolerance of osteoporotic bone, resulting with fracture at this critical interface and loosening of the implant[23].

In addition to mechanical fragility, a disturbance in the process of bone healing and implant osseointegration has been proposed to be another source of poor surgical outcome in osteoporotic patients. Osteoporotic patients have been observed to take an average of 20% longer to achieve bony union compared to controls when treated operatively for femoral diaphysis fractures[24]. Furthermore, osteoporotic patients who sustain unstable proximal femur fractures were found to be twice as likely to fail fracture fixation when compared to non-osteoporotic controls[25]. Interestingly, osteoporosis alone has not been found to be an independent factor for the development of a bony nonunion[26]. A possible explanation for this finding is that although osteoporotic fractures have the biological ability to eventually heal, the healing process is delayed and is

structurally incompetent in its development, leading to physical collapse, implant failure if surgery has been performed, and poorer functional outcome. This hypothesis has been strengthened by the histological finding that callus formed following osteoporotic vertebral fractures in humans was found to be in various stages of matrix synthesis, bone formation, and bone remodeling[27], suggesting that compared to normal fracture callus, the callus formed by osteoporotic bone is more fragile and susceptible to refracture, prolonging the time to which structural integrity is reached.

The precise mechanisms responsible for delayed bone healing and implant osseointegration in humans have yet to be described. However, a growing interest in understanding the biology of osteoporosis and attempting to improve clinical outcomes has led to the development of animal models in order to improve the integration of orthopaedic implants to poor quality bone. However, each model differs in the manner by which it represents bony fragility in humans.

1.4 – Current Animal Models of Poor Bone Quality

1.4.1 – Choosing an Appropriate Animal Model

Animal models vary significantly in their ability to reproduce mechanical and biological characteristics of human bone. Larger animals such as sheep and pigs exhibit intracortical remodeling during fracture healing and have Haversian systems which closely resemble human bone[28]. However, the bones of these animals also exhibit a brick-like ‘plexiform’ pattern that has few pores and, while beneficial in protecting the growing animal from fragility fractures, makes

comparison with osteopenic human bone difficult[29]. Due to this limitation, as well as the expense of housing large animals, rodents comprise the majority of models of poor bone quality. Although rats and mice lack Haversian systems, they instead utilize resorption cavities for bone remodeling, a process which has found to be similar to what is observed in larger animals[30]. Furthermore, the difference in bone properties between osteopenic animals and controls does not significantly change when comparing larger animals to rodents[31]. This finding indicates that rodent models are equally as appropriate to analyze bone healing in osteopenic bone as large animal models. In addition, the ability to manufacture gene-targeted mouse models as well as suppress genetic expression through use of antibodies permits study on the molecular mechanisms of rodent bone healing that are simply not possible to yet perform in larger animals.

Three of the most commonly utilized models of poor bone quality are subsequently discussed. The insight each model has provided into the clinical problem of osseointegration of implants to osteopenic bone is discussed. Furthermore, model-specific studies on fracture healing are briefly summarized to further elicit abnormalities in bone biology.

1.4.2 – Models Representing Post-Menopausal Osteoporosis

The animal model that has been most studied for osteopenic bone has been the ovarectomized rat. Through removal of the ovaries, endogenous estrogen levels are minimalized, reproducing a menopausal state which has been shown to produce changes in cancellous bone that are similar to changes

observed in humans[28]. If this is not performed, rodents otherwise do not become menopausal, even in advanced age[32]. Estrogen's role in bone density maintenance is believed to be due to indirect inhibition of osteoclastogenesis, and direct inhibition of osteoclast function[33]. Therefore its absence promotes osteoclast formation and activity. The ovarectomized mouse, as in osteoporotic human bone, has been shown to have delayed bone healing capabilities, with smaller, less mineralized callus[34]. Additionally, ovarectomized rodents demonstrate poor remodeling capabilities with lower tolerance to tensile stress compared to non-ovarectomized controls[35].

The presence of estrogen, administration of bisphosphonates, and coating of implants have been identified as having significant effects on osseointegration in ovarectomized animals. Giro and colleagues observed that ovarectomized Wistar rats exhibited significantly less osseointegration of a metaphyseal tibial implant compared to controls[36]. Similar results have been found in a ovarectomized sheep model[37]. Treatment of ovarectomized rats with bisphosphonate therapy has been shown in dental implants to improve ossteointegration and well as increase bone mineral density of peri-implant bone[38]. Such benefits from bisphosphonate therapy in are reflected in the human literature for post-menopausal osteoporosis, with bisphosphonates such as alendronate, risendronate, and zolendronic acid being shown to reduce the risk of fracture from minor to moderate trauma to all skeletal sites by 30-50% and multiple vertebral fractures by 90%[39]. The metal the implant is made of as well as what it is coated with also affects osseointegration. Rocca and colleagues

showed in ovarectomized sheep that tibial diaphyseal screws were better osseointegrated histologically if the implant was made of titanium versus stainless steel[40]. Furthermore, coating the implant with hydroxyapatite improved osseointegration for both titanium and stainless steel implants, with no significant difference found between them.

Although the ovarectomized animal model has provided insight into potential mechanisms of impaired fracture healing in osteopenic bone, it has several limitations with regard to being a true representation of human disease. Firstly, the decrease in bone mineral density following ovariectomy is not as significant as what is observed in humans[28]. The ovarectomized rat exhibits an atypical pattern of bone loss, with a rapid loss in bone mineral density observed in the first 100 days and then relative stabilization for the following nine months[41]. This is in contrast to post-menopausal human women, whose steady, progressive loss in bone mineral density predisposes them to higher incidences of fragility fractures as they get older. Furthermore, the osteoblasts produced by ovarectomized rats function normally, unlike human osteoblasts, which proliferate and metabolize at a decreased rate in the absence of estrogen[42]. With regard to larger animals, the ovarectomized canine shows no decrease whatsoever in bone mineral density, making its use controversial[43]. Also, as in humans, bone mineral density varies in large animals according to light exposure and seasonal conditions[44]. Therefore, the time of the year in which an experiment is performed could affect results in these models.

1.4.3 – Models Representing Age Related Decline in Bone Quality

Senile osteoporosis in humans, specifically in males, is related to age-related changes in bone cellularity which are not hormonally driven and therefore are not sufficiently presented by ovarectomized animal models[45]. Compared to pediatric bone, comprised of highly cellular and vascularize periosteum, older bone is characterized by decreased cellularity and slower differentiation brought about by undetermined mechanisms[46]. This decline in cellularity has been shown to have a deleterious effect on fracture union in rats. Meyer and colleagues showed in a stabilized femur fracture model that 32-week old rats took 1.5 times longer to regain fracture stability compared to 8-week old rats, while 50 week old rats did not regain mechanical stability up to six months post injury[47]. In mice, the most widely utilized advanced age model is the C57BL/6J mouse, aged 12 months or longer. Mechanical and histological evaluations have revealed that these mice undergo changes in mechanical strength and cellularity similar to those observed in humans[48]. However, these changes are gender specific, with female C57BL/6J mice exhibiting more pronounced age-related declines in vertebral and distal femoral trabecular bone volume compared to males[49].

No study to date has directly examined osseointegration of aged C57BL/6J mice. Nevertheless, investigations into fracture union as well as osseointegration in young C57BL/6J mice have provided interesting results. When comparing old to young C57BL/6J mice, Naik and colleagues observed delayed union in one-year old female mice six weeks following fracture, with poor chondrogenesis, delayed callus vascularity, and decreased COX-2 expression

within the callus[50]. This last finding is of interest since it suggests that alterations in the inflammatory response to fracture healing due to age may be partially responsible for slower fracture healing. Work by Chikazu and colleagues suggest that COX-2 expression may also be important for osseointegration. In their study, young C57BL/6J mice treated with intramedullary femoral implants, COX-2 knockout animals produced poor peri-implant bone formation. Meanwhile, wild type animals produced robust amounts of peri-implant bone with, most significantly, high COX-2 expression within the peri-implant bone[51]. This result indirectly suggests that age related delay in implant osseointegration may be in part due to a poorly regulated inflammatory response.

An alternative to waiting for rodents to age is to accelerate the aging process. The senescence-accelerate mouse (SAMP6) developed in Japan is an often used model for age related poor bone quality[52]. These mice exhibit decreased amount of osteoprogenitor cells in their bone marrow as early as 4 months of life and have age-related decline in bone mineral density[53]. Mesenchymal stem cells, the precursors to osteoblasts, have been found to act similarly to those in osteoporotic humans, having a reduced tendency to undergo osteoblast differentiation in SAMP6 mice[54]. With regard to osseointegration, the only study to date demonstrated that SAMP6 mice are able to create peri-implant bone around bicortical titanium coated plastic implants, but the density of this bone was up to 40% lower compared to controls within the medullary canal[55]. Bone mineral density of cortical bone around the implant did not differ between the groups, suggesting that implants placed in osteopenic bone should have

some form of cortical contact to ensure purchase and stability. The SAMP6 mouse is a useful representation of age related senile osteoporosis and is derived, like the subsequent models, from targeted gene mutations.

1.4.4 – Why Develop Models Derived from Targeted Gene Mutations?

Animal models involving targeted mutations of genes encoding known regulators of skeletal development have been informative in revealing the specific role growth factors play in osteogenesis. This is not surprising since up to 70% of individual differences in skeletal development, remodeling and the age-related decline in regenerative capacity is genetically determined. Examination of genetic expression during rodent fracture healing has revealed that similar genetic events during osseointegration and fracture healing, with bone morphogenetic protein (BMP) 2, fibroblast growth factors (FGFs), osteocalcin and vascular endothelial growth factor (VEGF) being some of the many participants in both processes[56]. Recent investigations have determined that differential expression does occur depending if an implant is utilized for fixation. Recently, Ogawa & Nishimura demonstrated that three genes, apoplipoprotein E, prolyl 4-hydroxylase alpha-subunit and an unknown transcript were uniquely expressed specifically when titanium implants were implanted into rat femurs[57]. This expression increased with textured implants were utilized and decreased in estrogen deficient animals, suggesting that these genes could have regulatory roles in osseointegration. Targeting these genes and others important in both fracture healing and osseointegration through knockout/knockdown models is the next logical step.

One such model involving a gene important in skeletal development and fracture fixation is the fibroblast growth factor receptor (FGFR) 3 knockout mouse.

1.4.4.1 – The Fibroblast Growth Factor 3 Receptor Knockout Mouse Model

Fibroblast growth factors (FGFs) are a large family of polypeptides composed of 22 members in humans[58]. FGFs have a high affinity to heparin sulfate, binding to it in order to activate one of four FGFRs. The third FGFR, FGFR3, has been implicated in enchondral bone development and has also been identified in fracture healing. FGFR3 can be activated by several ligands, including FGF1, 2, 4, 8, 9, 17, 18, 19 and 20[59].In postnatal life, FGFR3 is found in pre-osteoblasts and osteoblasts, and has been shown to upregulate osteoblast differentiation[60]. FGFR3 expression following fracture has been shown to be present in hypertrophic chondrocytes found within fracture callus[61], with expression rates peaking at 9-10 days post fracture[62]. This peak suggests FGFR3 signalling is involved in the transition from resolving chronodrogensis and the initiation of osteogenesis. The development of an FGFR3 knockout ($FGFR3^{-/-}$) mouse has provided greater insight into the role of FGFR3 signalling. Targeted inactivation of the FGFR3 gene produces overgrowth of the axial and appendicular skeleton in utero[63,64] as well as osteomalacia, osteopenia and osteoarthritis in skeletally mature mice[65,66]. The FGFR3c isoform was later shown to be responsible for these skeletal defects[67]. Adult FGFR3-deficient mice therefore exhibit skeletal defects similar to those seen in the aging human skeleton and their bone marrow cells exhibit atypical proliferation and

differentiation behaviour compared to wild type controls[68]. These findings justify the use of the FGFR3$^{-/-}$ mouse as a useful model for studying the effects of fibroblast growth factors on bone formation and osseointegration in an environment of osteopenic, poor quality bone

1.4.4.2 – The FGFR3 Ligand of Interest: Fibroblast Growth Factor 18

Of the ligands that bind to FGFR3, fibroblast growth factor (18) is of specific interest due to its potential therapeutic role in fracture healing and osseointegration. In the growing mouse skeleton, FGF18 is important in promoting chondrocyte proliferation and differentiation[69], as well as promoting vascularization to bone, and recruiting osteoblasts and osteoclasts to bony growth plates[69-71]. During fracture healing, FGF18 expression peaks at 4-9 days post fracture, suggesting an importance in the transition from chondrogenesis to osteogenesis that occurs in tandem with peak FGFR3 expression[62]. Although no study to date has examined FGF expression uniquely during implant integration without fracture, similar participants as in fracture healing have been detected, indicating FGF18 likely has a role in bone formation involved in osseointegration. This role may occur through FGFR3 signaling, or, as recent work has suggested, through an alternate receptor.

Investigations of the FGF18 knockout mouse model has produced indirect evidence that FGF18 may signal to an alternate FGFR and that such alternative signaling may induce osteogenesis. When comparing FGF18$^{-/-}$ and FGFR3$^{-/-}$ mice, Liu and colleagues noted that both models produced abnormal growth

plates with similar features of expanded proliferating and hypertrophic zones[69]. This finding suggested that FGF18 mediated FGFR3 signaling inhibits chondrocyte proliferation and differentiation. However, $FGF18^{-/-}$ mice expressed delayed ossification that was more severe than in $FGFR3^{-/-}$ mice. Furthermore, abnormalities in cranial periosteum and endosteum were found in the $FGF18^{-/-}$ mice. These unique findings in the $FGF18^{-/-}$ mice are indirect evidence that FGF18 signals through a different FGFR, potentially FGFR1 or 2. These two FGFRs are likely candidates due to their similar roles in skeletal development: FGFR1 regulates osteoblast maturation of osteoprogenitor cells throughout development[72], is expressed immediately following a fracture and continues to rise thereafter[62]. FGFR2 affects skeletal growth and bone mineral density[73], is believed to be a positive regulator of ossification[74], and is expressed in fracture healing in a similar pattern to FGFR1[62]. FGF 18 has been identified as an important mediator of bone biology in vivo and further understanding of its function in the presence and absence of FGFR3 would assist in determining if it has clinical application in the osseointegration of poor quality bone.

2.0 – OBJECTIVE OF STUDY

The objective of this thesis was to determine the in vivo and in vitro effects of FGF18 on osteoblastogenesis and osseointegration in the presence and absence of FGFR3. In vivo, we monitored the effects of exogenous administration of FGF18 on bone formation and osseointegration of a biocompatible intramedullary implant in $FGFR3^{+/+}$ and $FGFR3^{-/-}$ mice. These

effects were quantified using high resolution micro-computed-tomography (μCT) to measure several bone morphometric indices and histological examination to interpret and confirm radiological findings. In vitro, we examined how proliferation and differentiation of mesenchymal stem cells changed depending on the presence or absence of FGFR3, the administration of FGF18, and the concentration of FGF18 administered. Such comparisons were made using fluorescence metabolic assay, cell counting and histomorphometry.

Results demonstrate that FGF 18 treated femurs produced greater peri-implant bone formation in both wild type and $FGFR3^{-/-}$ mice, as well as less fibrous tissues in $FGFR3^{-/-}$ mice. In-vitro work showed that FGF 18 increased MSC proliferation in both wild type and $FGFR3^{-/-}$ MSCs, and inhibited differentiation in wild type MSCs.

3.0 – MATERIALS AND METHODS

3.1 – Mice

All animal procedures were performed in strict accordance with protocols approved by a McGill University review board, which are based on those set by the Canadian Council on Animal Care. All mice used for this study were obtained from in-house breeding of FGFR3+/- mice maintained for more than 20 generations on a C3H background. Although FGFR3+/- mice on a Bl6 strain are also available from Washington University, the C3H mice maintain the same skeletal phenotype as Bl6, are more amenable to handling and can tolerate interventional orthopaedic procedures.

3.2 – Implant fabrication

Nylon fishing line of 0.4mm diameter (Pure Fishing 1900, Spirit Lake, Iowa) was cleaned by sonication for 30 minutes in 1%:1% Renuzyme (Getinge, NY, USA) and Liqui-Nox (Alconox, NJ, USA) at 50°C, followed by 2% NaOH at 21°C and rinsing three times with distilled H2O at room temperature. The line was then placed in a vacuum and underwent further cleaning through high pressure oxygen plasma etching. Titanium was chosen to coat the implant due to its clinical use and known biocompatibility with bony surfaces[75]. A uniform 200nm layer of commercially pure titanium was deposited on the line using physical vapor deposition (PVD), a technique utilized in medical applications due to the ability to perform it at low temperatures using inert substances. The PVD process involves ionized gas (Argon) striking a cathode within a vacuum environment. Upon striking the cathode, titanium particles are released, travel across the vacuum space and condense on the target surface. Using a similar methodology previous described[76], each nylon implant was placed in the PVD chamber, the chamber was warmed with radiant heaters at 140°C, and the chamber was backfilled with pre-purified 99.99% pure argon at pressure of 2.0 Pa. Titanium was evaporated from a commercially pure source with an arc current of 125 A. In order to establish a coating thickness of 200nm, a current of 1.5A was applied in order to ionize the Argon gas, which subsequently bombarded the titanium source, causing titanium particles to travel and coat the nylon implant. After coating the titanium, the next step was to ensure that a smooth topographical

surface devoid of significant roughness had been produced.

Surface topography of the titanium-coated lines was quantified as described previously[77] using a VEECO NT8000 WLI (Veeco Metrology Inc, Tucson, AZ) instrument in Vertical Scanning Interferometry mode. Using a vertical resolution of 1nm, 5 images of each surface were obtained using a x50 objective with a x0.5 field of view, at a resolution of 640 x 480 pixels. The data was fitted to a best fit cylindrical spline function. The average variation in magnitude of surface structures for all titanium coated lines was 0.8 μm, a value consistent with non-textured smooth commercial implants[78].

The titanium-coated lines were then placed in an aseptic environment and cut to 10mm lengths for implantation. The night prior to surgical procedure, all implants were sterilized overnight under UV irradiation and then immediately prior to implantation, all implants were immersed in 70% ethanol and then rinsed three times with sterile PBS.

3.3 – Developing an Intramedullary Implant model in the C3H Mouse

Several challenges arose when developing a surgical technique to safely and consistently insert intramedullary implants in mice used for study. The small stature of the C3H mouse, its femur (Figure 1a), and consequently its miniscule circulating blood volume meant that dissection needed to be limited in order to prevent accidental exsanguinate or devascularisation of the bone. Furthermore, the increased curvature and fragility of the FGFR3$^{-/-}$ femurs meant that accessing the femoral canal using rigid instruments such as drill bits or Kirschner wires

would likely cause a complex fracture which would be impossible to immobilize. Initial efforts involved using a retrograde approach whereby an incision was made over the knee and the implant was inserted through a hole made in the distal femur between the femoral condyles up into the proximal femur. Although this approach permitted a small incision, there was no way to intraoperatively confirm that the implant had not penetrated the diaphyseal cortex proximally. Therefore, we devised an antegrade approach similar to what is surgically performed in humans, in which the implant is inserted in the proximal femur adjacent to the femoral head. We preferred this approach because it does not disturb the hip or knee joint, permits for easier insertion of the implant due to less curvature in the proximal femur, and has better soft tissue coverage of the insertion site.

3.4 – In-vivo Administration of FGF 18 & Surgical Procedure

Nine $FGFR3^{-/-}$ and five $FGFR3^{+/+}$ mice, all male and aged 8 to 10 months received bilateral intramedullary femoral implants. For each mouse, the lower back and lateral thighs were shaved. Then, under induction and maintenance of inhaled vaporized isoflurane, shaved areas were washed with 2% chlorhexidine and the animals were transferred to a sterile operative field. A 5mm skin incision was made bilaterally over the proximal hip and gentle subcutaneous dissection was performed. The rodent equivalent of the short external rotator muscle group of the hip were incised longitudinally in order to expose the greater trochanter of the femur and proximal femoral metaphysis (Figure 1B). The rodent equivalent of the piriformis fossa, which is utilized in humans as a surgical landmark for

intramedullary access to the femur, was identified. A 25 gauge needle was then inserted slightly medial to the greater trochanter, within the equivalent of the piriformis fossa, in a direction parallel to the femoral diaphysis (Figure 1C). Due to the anterior bow of the rodent femur, significant care was taken to visualize the femoral shaft underneath the quadriceps muscles to ensure the syringe did not penetrate the diaphyseal cortex. Upon removing the needle, a 1710 Microliter syringe (Hamilton Company, Reno, NV) was inserted through the same hole in order to inject 10µl of solution, either FGF 18 or control (Figure 1D). To standardize treatment for each mouse, all left femurs received 0.5µg of recombinant FGF 18 (MW = 19.83 x 10^3 KDa, Merck Serono, Switzerland) in 10µl of sterile saline. Right femurs received 10µl of sterile saline only to serve as a control. Following the injection, 10mm a titanium-coated nylon implant was inserted (Figure 1E). The overlying muscle and skin were then re-apposed using 5-0 resorbable Vicryl sutures in separate layers.

All animals were provided with subcutaneous analgesia immediately following surgery and on the first three postoperative days. Following a 6 week postoperative period in which animals were allowed free access to food and water, they were euthanized and their femurs were harvested for analysis. Freshly isolated femurs were dissected free of soft tissue and an osteotomy was made at the distal third of the femur. Femurs were then fixed with 4% paraformaldehyde for 24 hours at 4°C and then washed twice with PBS for 48 hours.

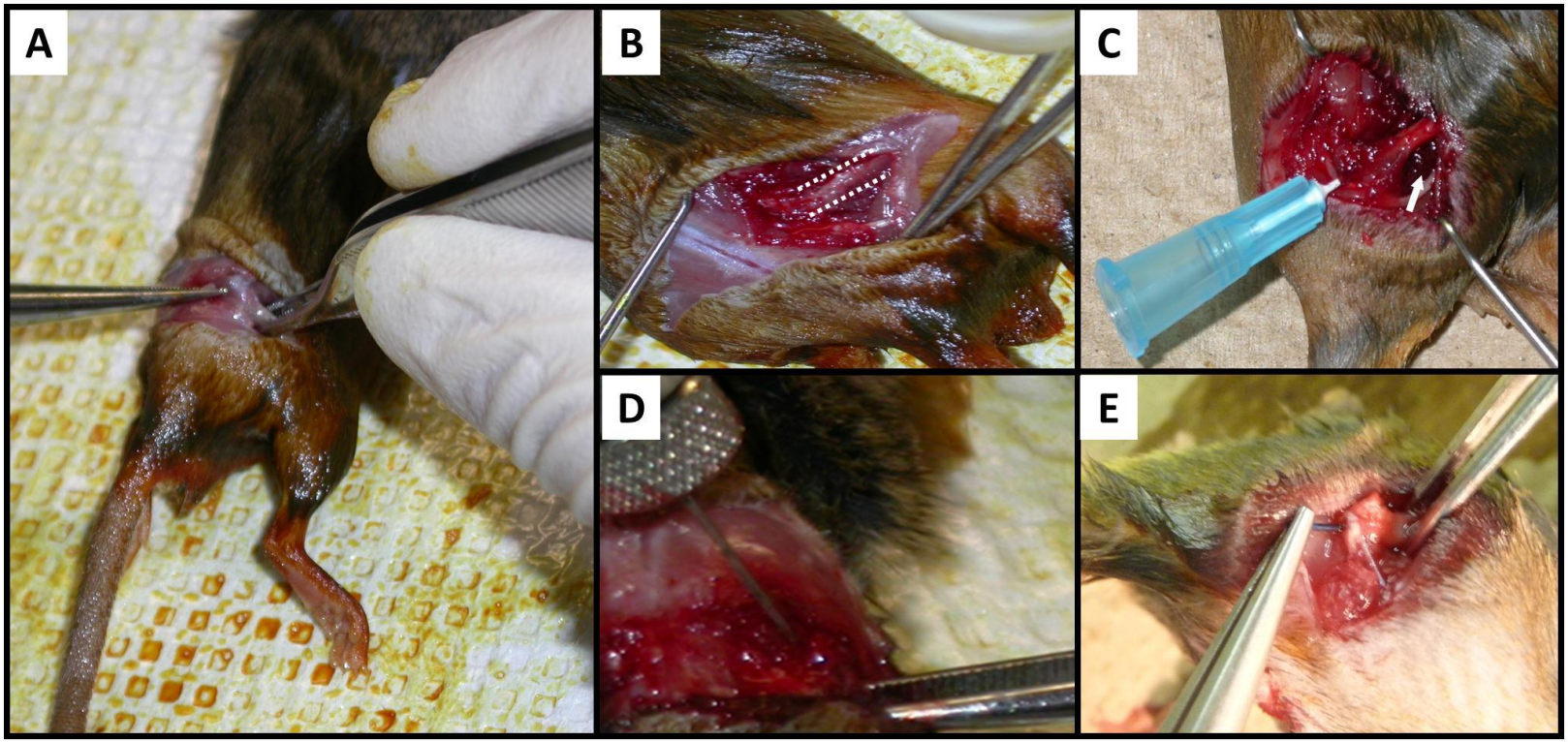

Figure 1: Photographs demonstrating surgical implantating of intramedullary titanium coated titanium implants via an antegrade approach. **A**: Under isoflurane anesthesia following shaving of overlying fur and preparation with poviodine, a 3cm incision was made over the hip joint in line with the femur. **B**: The short external rotators are incised longitduinally, exposing the proximal femoral canal (white dotted lines). **C**: A 25-gauge needle is inserted medial to the greater trochanter in a recess similar to the piriformis fossa found in humans. The proximal femoral diaphysis is inspected (solid white arrow) to ensure the needle has not perforated cortical bone. **D**: A Hamilton syringe is then inserted and 10µl of either FGF 18 or sterile saline into the medullary canal. **E**: A 10mm long titanium coated nylon rod is then carefully inserted into the medullary canal. The muscle, soft tissue and skin is apposed with 5-0 Vicryl suture.

3.5 – Micro CT analysis of peri-implant bone regeneration

Micro computed-tomography (μCT) scanning was performed on each harvested femur using a Skyscan1172 instrument equipped with a 1.3 Mp camera (Skyscan, Kontich, Belgium). Using an energy source of 80kV and 100 μA, images were captured at a rotation step of 0.45º between frames using a 0.5mm Aluminum filter at a magnification of 5μm per pixel. 2-dimensional serial cross sections were assembled into 3D reconstructions and analyzed using Skyscan software (CTAn version 2.0.0.1) supplied with the instrument.

Upon identifying the intramedullary implant, a ring-shaped region of interest was drawn expanding 30μm outwards in order to assess peri-implant bone formation (Figure 2A-C). This ring shape of peri-implant tissue was measured over a 0.5mm metaphyseal segment of bone extending from the lesser trochanter distally. This segment was chosen since the majority of fragility fractures which heal poorly tend to occur in metaphyseal bone. A threshold of 40% maximum grayscale (80/200) was used to segment bone from non-bone.

Five morphometric indices measuring bone volume and bone connectivity were measured from the binarized 3-dimernsional volume of interest. Indices of bone formation, including percentage of bone volume (BV) relative to the total VOI and the trabecular number was measured. With regard to the structural integrity of the bone formed, the structural model index, based on the relative prevalence of rods and plates in a 3d space[79], and trabecular pattern factor, an inverse index of connectivity based on the convexity and concavity of bony surfaces[80], were measured. Finally, the intersection surface[81], which quantifies

the amount of bone coming into contact with the adjacent intramedullary rod, was measured.

3.6 – Histological observation of peri-implant bone regeneration

Following µCT analysis, femurs were embedded in a mixture of methylmethacrylate and glycolmethacrylate. Specimens were dehydrated in graded alcohols from 70% to 100%, before vacuum infiltration and embedding in resin. 5µm sections of proximal metaphyseal bone were cut on a modified Leica RM2265 rotary microtome (Leica Microsystems, Richmond Hill, Canada) and stained with 5% silver nitrate for 30 minutes under ultraviolet light, then with 0.2% toluidine blue for 1 minute as described previously[65].

Staining of serial sections for Toluidine Blue and Von Kossa (VK) was performed according to the manufacturer's instructions using naphthol AS-TR phosphate (Sigma-Aldrich, Oakville, Ontario) as described previously[65]. Additionally, slides were stained for alkaline phosphatase and tartrate resistant acid phosphatase at 37°C in a Coplin jar placed in a waterbath. Briefly, sections were rinsed with aqueous 20% sucrose, rinsed and incubated for 60 minutes in 50ml of 200 m*M* Tris-maleate buffer containing napthol AS-TR phosphate (Sigma-Aldrich) in 0.5ml *N*,*N*-dimethylformamide and 40mg Fast Blue RR salt. Additional rinsing with distilled water followed, with subsequent incubation for 30 minutes in solution containing acetate buffer, sodium nitraite, pararosaniline HCl solution, naphthol AS-TR phosphate in *N*,*N*-dimethylformamide and tartrate.

Slides were finally rinsed with distilled water, counterstained with 0.4% methyl green and mounted in an aqueous medium.

Digital images were captured at 10x and 40x magnification using an Axioskop 40 equipped with a AxioCam MRc camera (Carl Zeiss Canada Ltd, Quebec, Canada).Histological slides were then compared to axial µCT cuts.

3.7 – Administration of FGF 18 on Mitogenic and Osteogenic MSC Assay

Whole bone marrow was extracted from the tibiae and femurs of $FGFR3^{+/+}$ and $FGFR3^{-/-}$ mice all aged 10-12 months as described previously[82] and then plated in 10mm plates cultured with Alpha-Modified Eagle's Medium (AMEM) and 10% fetal bovine serum (FBS). Three days later, culture medium was changed and the plate was washed three times with PBS in order to remove nonadherent cells. Six days after harvesting, adherent cells were trypsinized, seeded at a density of 50,000 cells/cm^2 in 24-well plates and cultured again in AMEM and 10% FBS for 24 hours before entering either the mitogenic or osteogenic assays. For each assay, cells from three $FGFR3^{+/+}$ and three $FGFR3^{-/-}$ mice were utilized.

For the mitogenic assay, six different conditions were tested: In the four FGF18 conditions, cells were cultured in AMEM, 2% FBS and either 10^{-7}M, 10^{-8}M, 10^{-9}M or 10^{-10}M FGF 18. Furthermore, a positive control (AMEM+10% FBS) and a negative control (AMEM+2 FBS) with no FGF 18 were also included. For all conditions, culture medium and FGF 18 were replenished every three days. 3, 6 and 9 days following initial administration of FGF 18, cells were trypsinized and either transferred to a 96 well plate to undergo an Alamar Blue metabolic assay

(Trek Diagnostic Systems, Cleveland, OH) or were counted using a haemocytometer. Alamar Blue is a noncytotoxic agent which is reduced from a nonfluorescent blue to a pink fluorescent dye during the process of cellular metabolism. Changes in fluorimetry are assessed by a plate reader, with greater changes being indicative of greater metabolic activity.

For the osteogenic assay, cells were cultured in their respective 24-well plates until at least 75% confluent. Upon reaching confluency, AMEM was removed and replaced with osteogenic medium (10mM β-glycerophosphate & 50µg/mL ascorbic acid). In addition to osteogenic medium, cells were exposed to the same four FGF 18 conditions and two controls as used in the mitogenic assay. Culture medium and FGF 18 conditions were replenished every three days. 6, 9 and 12 days following initial exposure to FGF 18, plates were fixed in 4% paraformaldehyde for ten minutes and then stained with ALP and VK as described previously[68]. Following each staining, each 24-well plate was scanned at a resolution of 2400 dpi (V350, Epson America Inc.). From the large scanned image, individual wells were cropped into high quality 16-bit TIFF images. Dynamic histomorphometric analysis was performed by a single blinded individual using the Color Inspector plugin of the ImageJ software (Version 1.43 , Research Service Branch, NIH, USA) in order to quantify and compare percent osteoblast differentiation and mineralized bone formation.

3.8 – Statistical Analyses

In vivo data is representative of micro CT and histological data obtained from nine $FGFR3^{-/-}$ and five $FGFR3^{+/+}$ mice, with each mouse being considered

as a biological replicate. The in vitro mitogenic assay was performed in quadruplicate wells on three $FGFR3^{-/-}$ and three $FGFR3^{+/+}$ mice, with each replicate undergoing quadruplicate measurements in Alamar Blue and haemocytometer counting. The in vitro osteogenic assay was performed in quadruplicate wells on cells from three $FGFR3^{-/-}$ and three $FGFR3^{+/+}$ mice. Quantitative data is expressed as the mean $\pm$ standard deviation. All in vivo and in vitro data were assessed for being normally distributed using the Kolmogorov-Smirnov test and Shapiro-Wilk tests. As a result, parametric comparisons between three or more normally distributed groups were performed for in-vitro results using one-way analysis of variance. Levene's statistic and the Brown-Forsythe test were performed to assess similarity in variance. Post-hoc analysis was performed using Tukey's honest significance difference. Comparisons between non-normally distributed groups were performed with the Kruskal-Wallis one way analysis of variance and Mann-Whitney U test when necessary. A Bonferroni correction was applied to the critical *p* value, which was initially set at 0.05, when applicable.

4.0 – RESULTS

4.1 – Peri-implant osseous formation in $FGFR3^{+/+}$ and $FGFR3^{-/-}$ mice

μCT imaging permits extremely high resolution quantification and micro-architectural analysis of mineralized tissue, and has been used extensively in our laboratory for the phenotypic analysis of the developing murine skeleton. Peri-implant osseous formation was quantified in a ring-shaped region of metaphyseal

bone which measures 0.5mm long and which expanded 30μm outward from the intramedullary titanium implant (Figure 2A-C).

Grossly, $FGFR3^{-/-}$ femurs were shorter in length, had a bowed diaphysis and had dysplastic femoral heads in comparison to their wild type counterparts. Qualitative appraisal of 3-dimensional micro CT reconstructions. (Figure 2 D-G) indicated that FGF 18 treated femurs produced greater peri-implant bone compared to controls. Statistical analysis of bone morphometric parameters revealed that FGF18 treated $FGFR3^{-/-}$ femurs exhibited significantly increased percent bone volume ($p=0.015$) and trabecular number ($p=0.009$) compared to controls (Figure 3A, B). Furthermore, bony apposition to the intramedullary implant surface was also significantly increased ($p=0.031$) in FGF18 treated $FGFR3^{-/-}$ femurs (Figure 3C). $FGFR3^{+/+}$ femurs treated with FGF 18 demonstrated non-significant increases in percent bone volume ($p=0.117$), trabecular number ($p=0.347$) and implant apposition ($p=0.347$). Both $FGFR3^{+/+}$ and $FGFR3^{-/-}$ femurs demonstrated non-significant improvements in the connectivity of peri-implant bone, as represented by lower trabecular pattern factor ($p=0.347$; $p=0.233$) and structural model index ($p=0.347$; $p=0.508$) scores compared to controls (Figure 3D).

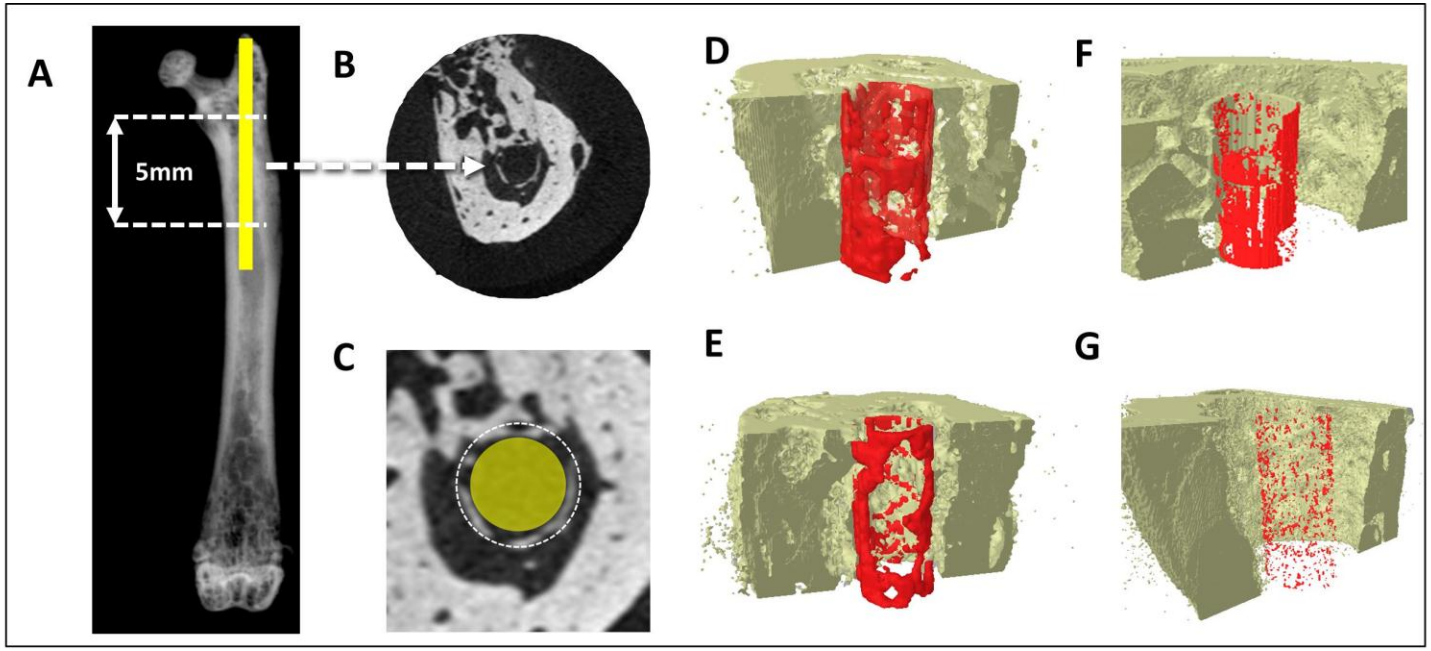

Figure 2: Schematic of antegrade titanium coated nylon rod inserted in the proximal femur of a wild type C3H mouse (**A**). 5mm of proximal femoral metaphysis was scanned with high resolution micro CT (**B**). Peri-implant bone formation was measured via a ring shaped volume of interest 30 µm expanding outwards from the implant (**C**). Three dimensional reconstructions of micro CT scans showed the peri-implant bone formation was nonsignificantly increased in FGF 18 treated $FGFR3^{+/+}$ (D) mice compared to controls (**E**). FGFR3 knockout mice treated with FGF 18 exhibited significantly greater peri-implant (**F**) comparedto control knockouts, who formed virtually no bone (**G**).

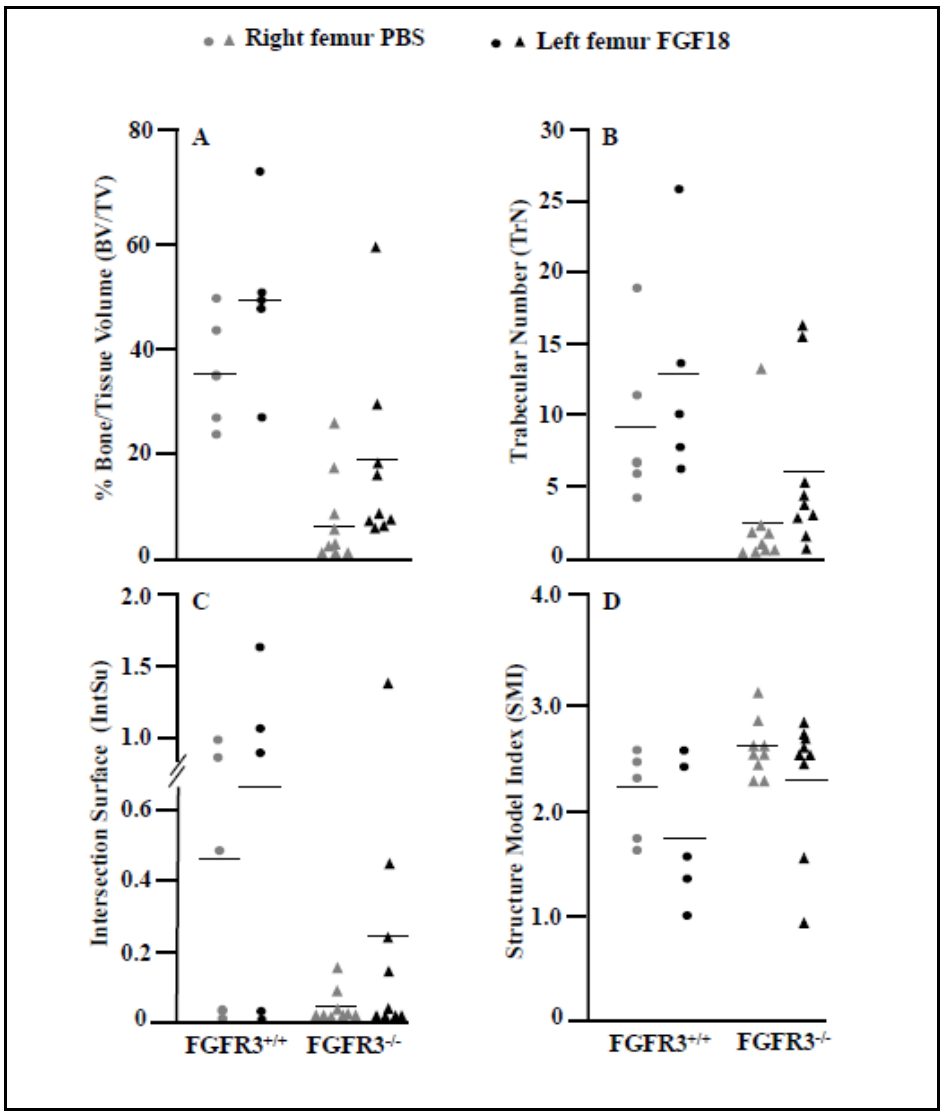

Figure 3: Quantitative micro CT analysis of FGF18 stimulated peri-implant bone formation. New bone surrounding the implants in the 2 mm x 30 micron ROI shown in Fig 1A was quantified in PBS treated (grey) and FGF18 treated (black) femora of 5 $FGFR3^{+/+}$ (circles) and 9 $FGFR3^{-/-}$ (triangles) mice using the Skyscan proprietary software CTAn 2.0.0.1. Scatter plots with mean values (line) are shown for percent Bone Volume relative to Tissue Volume (A), Trabecular Number (B), Intersection Surface (C), which is the point of contact between the implant and newly formed bone and the Structure Model Index (D), which is an index of the plate/rod like structures in trabecular bone. Significant differences in BV/TV ($p<0.002$), TrN ($p<0.03$) IntSur ($p<0.01$) and SMI ($p<0.05$) in the right PBS treated femurs of $FGFR3^{+/+}$ compared with $FGFR3^{-/-}$ mice. Treatment of the left femur of $FGFR3^{-/-}$ mice resulted in improvement in all parameters, which reached significance for BV/TV ($p <0.02$) and TbN ($p <0.02$). No significant differences were seen between left (FGF18) and right (PBS) femurs in $FGFR3^{+/+}$ mice.

Consistent with the micro CT data, von Kossa stained sections from the femurs of FGFR3+/+ and FGFR3-/-mice revealed more peri-implant bone in FGF18 treated left femurs compared with the contra-lateral PBS treated right femurs. Representative images of von Kossa stained sections from FGFR3-/- mice are shown in Figure 4. A sagittal section (A) shows sparse trabeculae and little bone apposition to the implant while higher magnification images of transverse sections of FGFR3-/- femurs revealed one of two general patterns shown in the upper (B, C) and lower (D, E) panels. In some mice, the femur treated with PBS exhibited a thick peri-implant ring of fibrous tissue (B) and normal marrow with minimal bone in the FGF18 treated femur (C). In others, the PBS treated femur looked similar to those of FGFR3+/+ mice with peri-implant bone and normal cellular marrow, but significantly more bone apposed to the implant in the FGF18 treated contra-lateral femur (E). Figure 5 shows serial sections cut through the PBS treated (B, D, F) and FGF18 treated (A, C, E) femurs of a third FGFR3-/-mouse, stained with von Kossa and toluidine blue (A, B), or for ALP to show osteoblasts (C, D) or TRAP to show osteoclasts (E, F). The increase in peri-implant bone in the FGF18 treated femurs (B) was accompanied by decreased and more focused ALP staining (D) and no apparent change in TRAP (F) compared with the PBS treated femur.

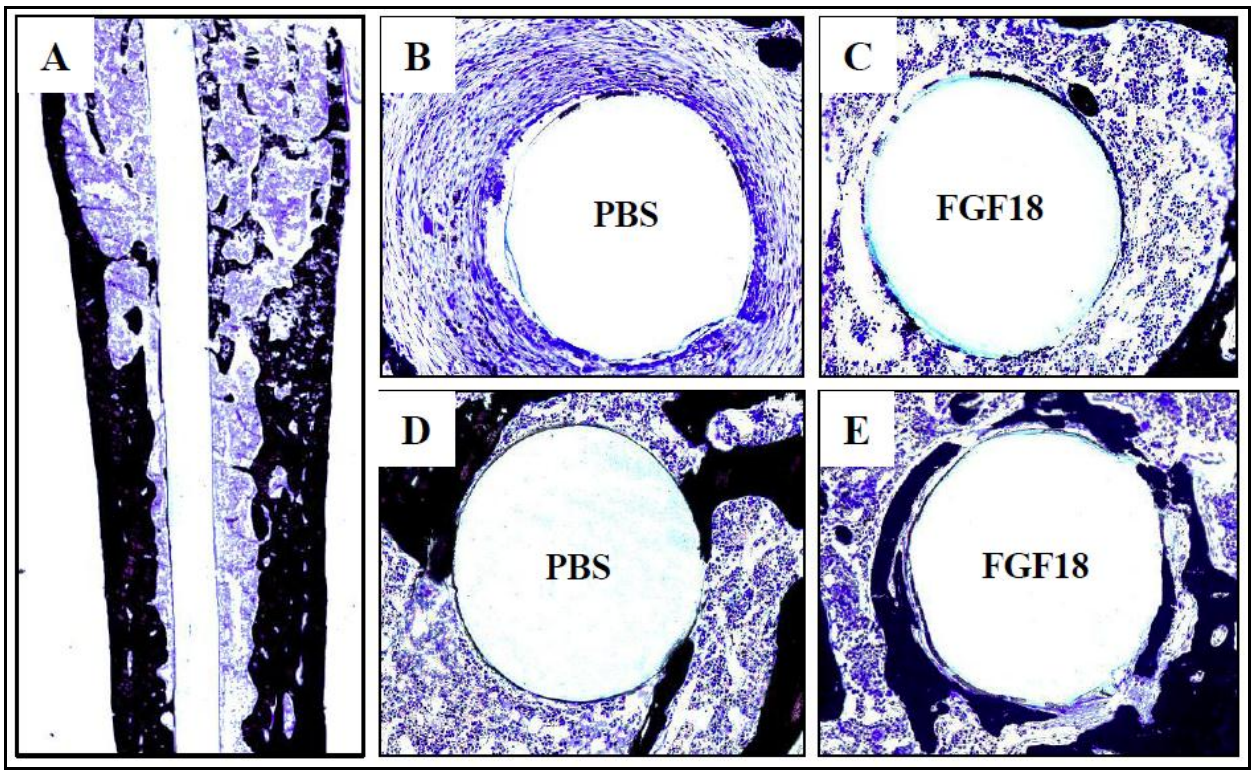

Figure 4: Histological analysis of FGF18 stimulated peri-implant bone in FGFR3$^{-/-}$ mice. To further examine the tissue response to FGF18 in FGFR3$^{-/-}$mice, femora were fixed in 4% paraformaldehyde, embedded in polymethylmethacrylate (PMMA) and 5 micron sections cut in the saggital (A) and transverse (B-E) planes. Under low power magnification (x2.7) trabecular bone was seen apposed to the implant in the metaphyseal region of the femur (A). Transverse sections (x20) from one mouse reveal a thick ring of fibrous tissue surrounded the implant in the PBS treated femur (B) and little bone but normal marrow in the contra-lateral FGF18 treated femur (C) The PBS treated femur of another mouse (D) showed normal marrow and bone but with a significant increase in bone in the FGF18 treated contra-lateral femur (E).

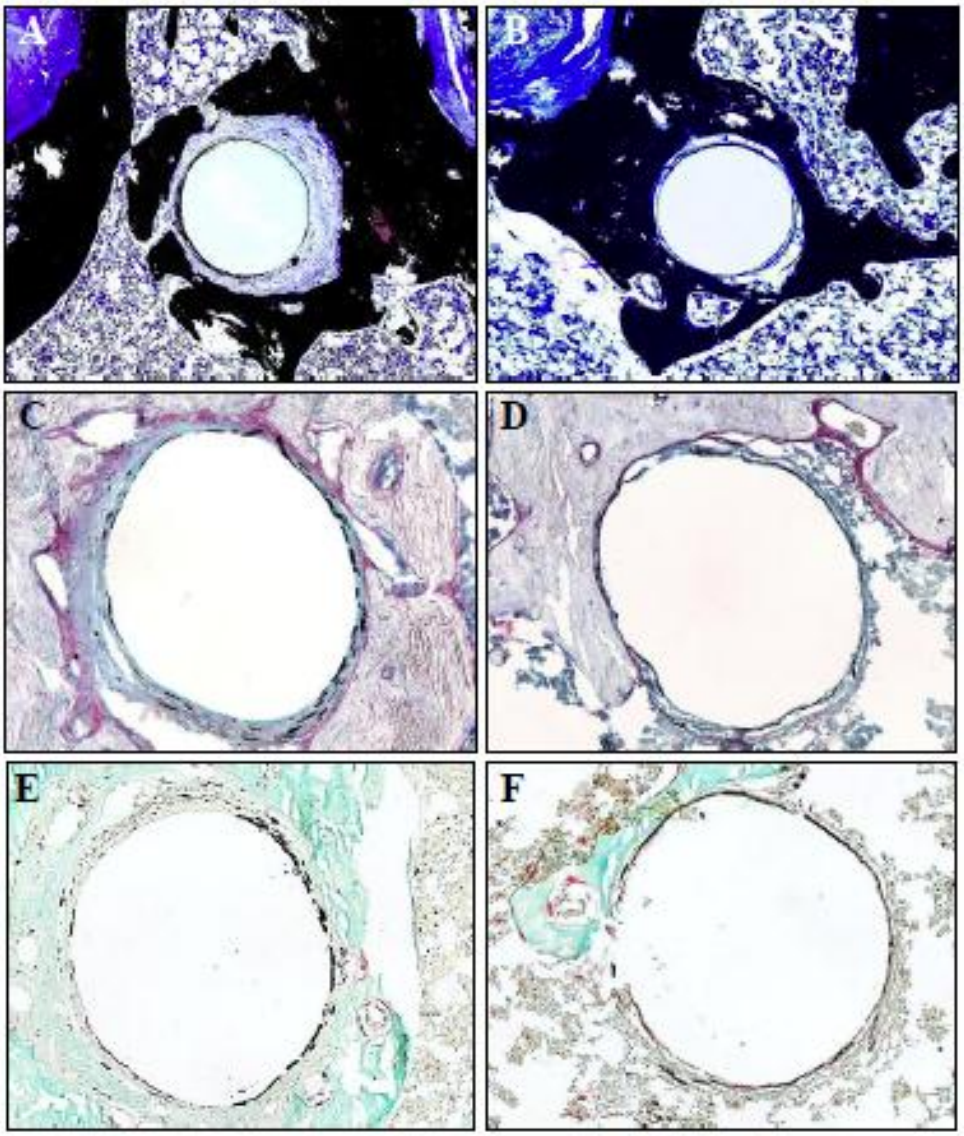

Figure 5: Bone cell activity in FGF18 and PBS treated femurs of FGFR3-/- mice. 5 micron transverse sections were cut in the 2 mm ROI from the left (0.5µg FGF 18) and right (PBS control) femurs of an FGFR3-/-mouse and stained with Von Kossa/Toluidine Blue to show morphology (A, B), alkaline phosphatase (ALP) for osteoblasts (C, D) and tartrate resistant acid phosphatase (TRAP) for osteoclasts (E, F). The PBS treated femurs exhibited a peri-implant ring of fibrous tissue (A), more ALP activity (C) and similar TRAP activity (E) compared to the FGF18 treated femur.

4.2 – Proliferation and differentiation of FGFR3$^{+/+}$ and FGFR3$^{-/-}$ MSCs

Following the finding that more, better connected bone was deposited in FGF 18 treated femurs in FGFR3$^{-/-}$ mice, mitogenic and osteogenic assays were conducted using bone marrow stromal cells (MSC) to determine if in vivo findings were influenced by alterations in function of these cells.

For the mitogenic assay, FGFR3$^{+/+}$ and FGFR3$^{-/-}$ MSCs treated with FGF 18 produced significantly increased ($p<0.001$) proliferation profiles compared to controls (Figure 6A, B). After 3 days, significant increases in cell counts were observed for FGFR3$^{+/+}$ cells treated with 10^{-7}M FGF 18, and FGFR3$^{-/-}$ cells treated with 10^{-7}M, 10^{-8}M and 10^{-9}M. At 6 days, significant increases in cell counts were again observed for FGFR3$^{+/+}$ cells treated with 10^{-7}M FGF 18, for and FGFR3$^{-/-}$ cells treated with 10^{-7}M, 10^{-8}M, 10^{-9}M and 10^{-10} M FGF 18. After 9 days, significant increases in cell counts were observed for FGFR3$^{+/+}$ cells treated with 10^{-7}M, 10^{-8}M and 10^{-9}M FGF18, for and FGFR3$^{-/-}$ cells treated with 10^{-7}M, 10^{-8}M, 10^{-9}M and 10^{-10} M FGF 18. No significant difference was found when comparing the cell counts of control FGFR3$^{+/+}$ and FGFR3$^{-/-}$ cells, indicating a similar inherent proliferation profile.

Changes in cellular metabolism in the proliferation assay were assessed through fluorescence changes observed in the AlamarBlue® assay (Figure 6C, D). For both FGFR3$^{+/+}$ and FGFR3$^{-/-}$ mice, significantly increased fluorescence was observed in three FGF18 treated conditions (10^{-7}M, 10^{-8}M, 10^{-9}M) at all three time points compared to controls ($p<0.001$). FGFR3$^{+/+}$ control cells showed a higher metabolic rate at all time points compared to FGFR3$^{-/-}$ controls ($p<0.001$).

Within groups, cells treated with 10^{-7}M and 10^{-8}M doses of FGF 18 exhibited significantly higher metabolic rates than 10^{-10}M at every timepoint ($p<0.01$).

In addition to proliferation, the effect of FGF 18 on osteogenic differentiation of $FGFR3^{+/+}$ and $FGFR3^{-/-}$ MSCs was investigated. MSCs plated at a high density were treated with osteogenic medium and the same four doses of FGF 18 as used in the mitogenic assay. The expression of osteoblast differentiation was detected through staining for alkaline phosphatase and quantified with histomorphometry using ImageJ software at 6, 9 and 12 days following FGF 18 administration. In control wells, alkaline phosphatase staining was positive in all conditions after six days culture in osteogenic medium. Histomorphometric analysis revealed that $FGFR3^{+/+}$ cells treated with FGF 18 produced significantly less alkaline phosphatase staining compared to controls after 9 days under one condition (10-7M, $p = 0.003$) and then all conditions after 12 days ($p<0.008$; Figure 6E). Conversely, in FGFR3-/- cells, no significant difference was noted throughout the differentiation experiment (Figure 6F).

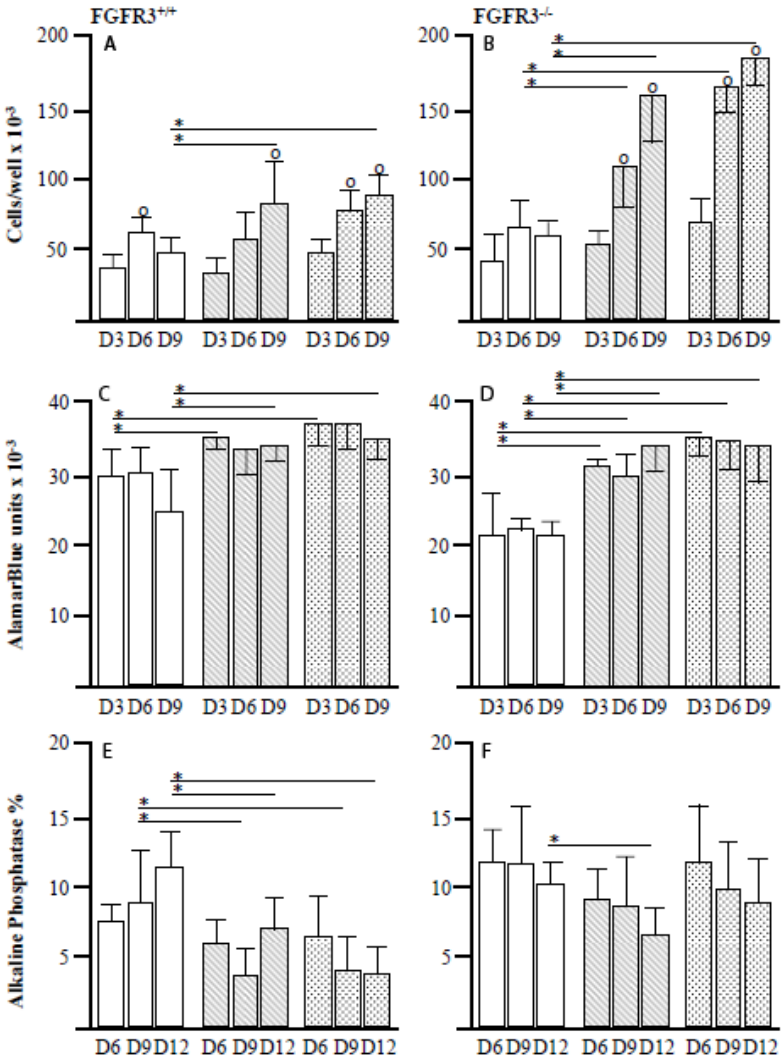

Figure 6: *Ex Vivo* response of FGFR3$^{+/+}$ and FGFR3$^{-/-}$ MSC to FGF18. MSC isolated from bone marrow harvested from the tibiae and femora of 10-12 month old FGFR3$^{+/+}$ and FGFR3$^{-/-}$ mice were plated at 50,000 cells/cm^2 in 24 well plates and grown in the presence of 2% FBS (white bars)), 2% FBS + 10^{-8} M (hatched bars) or 10^{-10} M (stippled bars) FGF18. Quadruplet wells were harvested at the indicated times for assessment of proliferation (A, B; Cells/well), metabolic activity (C, D; Alamar Blue) or differentiation (E, F; Alkaline Phosphatase). Time dependent increases in cell numbers were seen in cultures of FGFR3$^{+/+}$ and FGFR3$^{-/-}$ cells (o). Addition of 10^{-10} M FGF18 or 10^{-8} M FGF18 elicited a further increase compared with 2% serum alone (*), with a significantly more robust response in FGFR3$^{-/-}$ cultures. Metabolic activity was stimulated by FGF18 in cultures of FGFR3$^{+/+}$ and FGFR3$^{-/-}$ cells whereas ALP activity was marginally decreased. The results are representative of 3 biological replicates and are expressed as the mean ± standard deviations of four wells for each time point for each assay.

5.0 DISCUSSION

Our findings demonstrate that in a murine FGF receptor 3 knockout model, Fibroblast Growth Factor 18 augments peri-implant bone formation and osseointegration of smooth orthopaedic implants. Through micro CT analysis and histological observation, we show that when FGFR3 is absent, FGF 18 increases the amount of bone formed around a non-load bearing intramedullary implant, increases the number of trabeculae formed, increases bone-implant contact, and improves the structural qualities of the bone formed. Furthermore, FGF 18 prevents the formation of mechanically weak fibrous tissue that would otherwise form in FGFR3$^{-/-}$ mice. Fibrous overgrowth is proposed to be the end product of a chronic inflammatory response to a foreign body and poses a major barrier to the integration and biological performance of medical devices such as prostheses, implantable biosensors and drug delivery devices[83,84]. The fibrous response to implanted materials has been shown to involve the ubiquitous matrix protein fibronectin, which binds to the heterodimeric integrin cell surface[85]. Previous work in our group has shown that FGF 18 affects cellular adhesion to fibronectin and collagen substrates and that the regular MSC response to fibronectin is abnormal in FGFR3$^{-/-}$ mice[68,86]. Taking these findings into account, a potential explanation for the absence of a fibrous response in FGF 18 FGFR3-/- mice in the current study is due to a reversal of the altered recognition of fibronectin by bone marrow MSCs, leading to removal of the fibrous tissue via this cell population.

Our in-vitro studies demonstrate that one possible explanation for FGF 18's in-vivo bone forming effects is signaling through a non-FGFR3 mediated

mechanism. When FGFR3 is not present, FGF18 stimulates mesenchymal stem cell proliferation in a dose-dependent manner. Meanwhile, when FGFR3 is present, FGF 18's mitogenic effect of MSCs is substantially diminished and it also exhibits an inhibitory effect on osteoblastic differentiation. These findings, along with previous work showing that FGFR3 signaling inhibits chondrocyte proliferation and promotes differentiation[16,68,79], suggest that FGF18 mediated FGFR3 signaling does not play a prominent role in direct bone formation and instead is more directly involved with cartilage repair. A possible hypothesis linking FGFR3 signaling to eventual bone formation is that the formation of functional bone is preceded by cartilage, an ontogenetic pathway that has also been determined to occur during embryogenesis. Although peri-implant cartilage formation was not visualized in treated $FGFR3^{+/+}$ mice in this study, a subsequent investigation could be performed with earlier histological analysis to confirm if chondrogenesis precedes osteogenesis in wild type mice. What remains to be determined is whether the osteogenic effects of FGF 18 administration observed in our experiments arises through an alternative, unknown FGF 18 receptor, or through faulty FGFR3 signaling. We will explore the latter possibility first.

The effects of faulty FGF receptor 3 signaling have been extensively cited in the literature due to the association of specific FGFR3 mutations to musculoskeletal dysplasias including achondroplasia[87] and thanatophoric dysplasia[88], and oncogenic processes including multiple myeloma[81] and bladder cancer[89]. However, our current understanding of the role physiological FGFR3 signaling plays in bone repair has mainly arisen from observations in the

developing skeleton in FGFR3 knockout mice. Valverde-Franco and colleagues[65] demonstrated that although FGFR3$^{-/-}$ mice exhibited tibiae that were lower in bone mineral density, the number of mature osteoblasts within the bone were significantly higher than those observed in controls. Furthermore, these numerous mature osteoblasts exhibited a cuboidal morphology which differed from their flat, mineral producing wild type counterparts. These findings suggest that FGFR3 signaling initially inhibits precursor cell proliferation and osteoblast differentiation, a finding confirmed in the present work, and given its high expression in osteocytes[90], it may therefore be necessary for terminal maturation and bone matrix production. This dual role of FGFR3 in regulating terminal portions of chondrogenesis and osteogenesis can explain its upregulation in endochondral bone formation 10 to 14 days following fracture[91,92]. An alternative possibility of FGF 18's osteogenic effects is its signaling through another, unidentified FGF receptor.

With regard to identifying a potentially unknown pro-osteogenic FGF18 receptor, the literature indicates that both FGFR1 and FGFR2 are likely candidates. Increased FGFR1 expression has been determined to begin early on in fracture repair and peak at about 14 days following fracture, a pattern which coincides with that of FGF18[92,93]. Furthermore, Jacob and colleagues showed that FGFR1 accelerated differentiation of osteo-chondro-progenitor cells and was inversely related to FGFR3 expression in differentiated osteoblasts, a finding that could suggest that FGF 18 signals initially through FGFR1 and later through FGFR3 during fracture repair. FGFR2 has also been strongly implicated in FGF

18 signaling. FGF 18 treatment of primary articular chondrocytes was shown to cause an increase in proliferation and matrix production, as well as upregulating expression of FGFR2 and FGFR3[94]. Since FGFR2 is also known for its role for intramembranous ossification, the delayed intramembranous ossification observed in an FGF-18 deficient mouse, who otherwise exhibited phenotypes identical to an FGFR3 deficient mouse, suggests that FGFR2 is a downstream target of FGF 18 signaling[69]. Evidence suggesting that FGFR2 is a more promising candidate over FGFR1 arises from Olsen's surface plasmon resonance study indicating that FGF18 has a stronger binding affinity to FGFR2c over any FGFR1 variant[95], a finding also confirmed through FGFR-specific mitogenic assays[96].

This study does possess limitations. Firstly, the implant model utilized in the in-vivo experiments was not load bearing and did not involve the induction of a fracture. Load bearing implants are utilized for stabilization of fractures and joint replacements, and are subject to micromotion forces which occur as the animal ambulates. Furthermore, the formation of a fracture causes hematoma formation, macrophage invasion and degranulation of platelets, all acute processes that influence bone repair and do not necessarily occur in the current model. Another limitation was the lack of histological quantification of in vitro bone mineralization to confirm that increased osteogenic differentiation was associated with greater bone formation. Despite these limitations, this study corroborates in-vivo radiological and histological findings with in-vitro observations that lead to a credible hypothesis for FGF 18's role in bone formation. Furthermore, this study

provides the first methodology describing direct visualization of the osseointegration process both through radiographic and histologic means because the implant does not have to be removed during embedding and sectioning. Efforts are currently being conducted to reproduce the results from these experiments in load-bearing murine implant models as well as microarray investigation to further delineate the FGF-FGFR signaling process.

Collectively, evidence from the literature and the present work demonstrate FGF 18's versatility in signaling to multiple cellular targets to regulate bone formation. We have shown that FGF 18 improves osseointegration when FGFR3 is not present in an intramedullary implant model and that a potential mechanism may be through the enhancement of mesenchymal stem cell proliferation and differentiation through an alternate FGF receptor. Further research examining FGF 18's effects on FGFR-specific stem cells and osteoblasts could further clarify the non-FGFR3 signaling pathway that contributes to bone formation. Furthermore, additional translational studies employing FGF 18 and a compatible osteoconductive scaffold for use in a segmental fracture defect can further justify the use of FGF 18 for the increasingly prevalent problem of impaired bony repair.

6.0 FUTURE DIRECTIONS

In light of the results gained from our experiments, the possibility of utilizing the osteogenic effects FGF 18 through targeted gene therapy is being currently investigated. Through recruitment of host cell transcription machinery,

gene therapy leads to sustained local production of protein which is not immunogenic, therefore theoretically lasts longer than exogenously delivered protein. Viral-mediated cellular transfection is the most common method of introducing plasmid DNA into targeted cells, but concerns surrounding immunogenicity and mutagenesis[97] make it less appealing for fracture and osseointegration applications. The natural polymer chitosan has been used as an alternative for skeletal tissue applications because its nanocomplexes, which bind to plasmid DNA, have low immunogenicity, have intrinsic anti-bacterial properties and can also serve as a biodegradable scaffold that can be replaced with bone (11). Chitosan is produced by deacetylation of chitin, found in the exoskeletons of crustaceans, and its molecular weight and amount of deacetylation can be modified to alter its ability to protect the DNA it is carrying from nucleases (increased with high molecular weight and high deacetylation) and its ability to permit DNA to dissociate from it to interact with the intracellular transcription process (increased with lower molecular weight and low deacetylation)[98].

With the assistance of Drs. Micheal Buschmann and Marc Lavertu from École Polytechnique, an antegrade intramedullary implant model has been developed that delivers an FGF 18-chitosan mixture around an intramedullary implant. The FGF 18 plasmid is derived from the pVax1-FGF18 plasmid that is driven by a human CMV promoter. The study will be performed utilizing the same types of implant and surgical model as the previously described in-vivo FGF 18 protein experiment.

The first step is to validate the model by showing that a chitosan mixture remains in the intramedullary canal one week following surgery and that local genetic delivery occurs. To do so, two intramedullary solutions were prepared. The first, to show chitosan's presence in the intramedullary canal, consisted of chitosan complexed with rhodamine B isothiocyanate. The second, to show transfection, consisted of chitosan mixed with LacZ plasmid (p43LacZ). LacZ is the gene for beta-galactosidaase, and is a well-known method for identifying transfected cells in vivo[99]. In both solutions, chitosan with a molecular weight of 10 kDa and deacetylation rate of 92% was utilized, offering a balance of nuclease protection with transfection capability. Four adult FGFR3+/+ mice received bilateral intramedullary 10µL injections, with rhodamine-labeled chitosan injected in left femurs and chitosan/LacZ on the right. No implants were inserted. One week postoperatively, the animals were euthanized and their femurs harvested.

To detect the rhodamine-labeled chitosan, left femurs were fixed, washed twice in PBS, embedded in methymethacrylate and sectioned for viewing under fluorescent microscopy. To observe lacZ staining, all right femurs were fixed, immersed in 0.02% Glutaraldehyde in for 1 hour, washed in PBS, decalcified 4% EDTA over 2 weeks and then incubated in 0.1% X-gal, 2 mM MgCl2, 5 mM EGTA, 0.02% Nonidet P-40, 5 mM K3Fe(CN)6 and 5 mM K4Fe(CN)6 3H20 at 30˚C overnight. The femurs were then washed once in PBS, fixed at 4˚C overnight, then rinsed in 70% ethanol, embedded in paraffin wax, sectioned and counterstained with eosin.

Examination under fluorescent microscopy illustrated positive rhodamine signalling within the intramedullary canals of left femurs (Figure 7A). Examination of histological sections from the chitosan/LacZ treated mice revealed positive beta-galactosidase staining of marrow cells, suggesting successful LacZ transfection through chitosan (Figure 7B).

These preliminary results validate our current model of intramedullary gene delivery via a chitosan carrier. Future experiments will attempt to demonstrate successful FGF 18 transfection via chitosan in vitro using mesenchymal stem cells from $FGFR3^{+/+}$ and $FGFR3^{-/-}$ mice. Once transfection has been successfully shown, the next step will be to examine its effects in vivo.

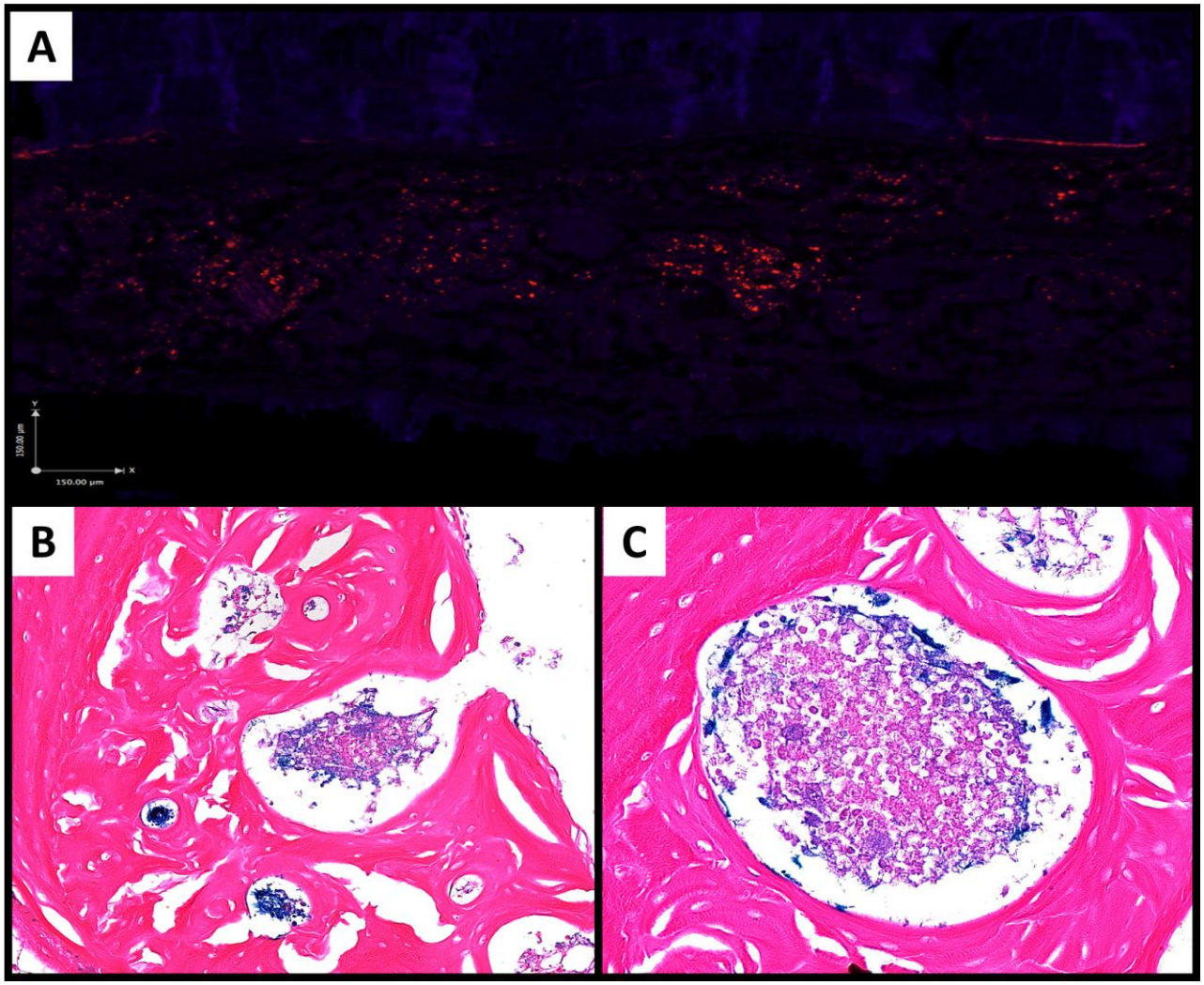

Figure 7: **A**: Superimposed fluorescence microscopy images of three wavelengths (380-420nm, 488-515nm, 590-617nm) taken of a 5 micron sagittal section of an FGFR3$^{+/+}$ mouse femur. The femur was harvested one week following intramedullary administration of rhodamine labelled chitosan (red). The section illustrates chitosan's continued presence with the medullary canal (blue). **B, C**: 5 micron axial sections taken from FGFR3$^{+/+}$ mouse femurs one week post administration of intramedullary chitosan/LacZ injections. Femurs were fixed and treated to optimize beta-galactosidase staining (blue). In both figures, positive staining is noted, suggesting that chitosan is successful in transfecting medullary cells via an intramedullary injection model.

REFERENCES

1. Licata A. Bone density vs bone quality: what's a clinician to do? *Cleve Clin J Med.* Jun 2009;76(6):331-336.

2. Delmas PD, Seeman E. Changes in bone mineral density explain little of the reduction in vertebral or nonvertebral fracture risk with anti-resorptive therapy. *Bone.* Apr 2004;34(4):599-604.

3. Weinstein S. 2010: the bone and joint decade. *J Bone Joint Surg Am.* 2000;82(1):1-3.

4. An Y. *Internal fixation in osteoporotic bone*: Thieme Medical Pub; 2002.

5. Gennari C, Martini G, Nuti R. Secondary osteoporosis. *Aging (Milan, Italy).* 1998;10(3):214.

6. Rosenberg AE. Bones, Joints, and Soft Tissue Tumors. In: Kumar V, Abbas AK, Fausto N, eds. *Robins and Coltran's Pathological Basis of Disease*. 7 ed. Philadelphia: Elsevier; 2005:1274-1286.

7. Dreinhöfer K, Anderson M, Feron J, et al. Multinational survey of osteoporotic fracture management. *Osteoporosis International.* 2005;16:44-53.

8. Patel RH, Lyles KW. Senile Osteoporosis as a Geriatric Syndrome. In: Duque G, Kiel DP, eds. *Osteoporosis in Older Persons: Pathophysiology and Therapeutic Approach*. London: Springer; 2008:71-81.

9. McCalden RW, McGeough JA. Age-Related Changes in the Compressive Strength of Cancellous Bone. The Relative Importance of Changes in Density and Trabecular Architecture*. *The Journal of Bone and Joint Surgery (American).* 1997;79(3):421-427.

10. Curtis R, Goldhahn J, Schwyn R, Regazzoni P, Suhm N. Fixation principles in metaphyseal bone—a patent based review. *Osteoporosis International.* 2005;16:54-64.

11. Cooper C, Campion G, Melton L. Hip fractures in the elderly: a world-wide projection. *Osteoporosis International.* 1992;2(6):285-289.

12. Gullberg B, Johnell O, Kanis J. World-wide projections for hip fracture. *Osteoporosis International.* 1997;7(5):407-413.

13. Burge R, Dawson-Hughes B, Solomon DH, Wong JB, King A, Tosteson A. Incidence and Economic Burden of Osteoporosis-Related Fractures in the United States, 2005–2025. *Journal of bone and mineral research.* 2007;22(3):465-475.

14. Bliuc D, Nguyen ND, Milch VE, Nguyen TV, Eisman JA, Center JR. Mortality risk associated with low-trauma osteoporotic fracture and subsequent fracture in men and women. *JAMA: the journal of the American Medical Association.* 2009;301(5):513.

15. Vestergaard P, Rejnmark L, Mosekilde L. Osteoporosis is markedly underdiagnosed: a nationwide study from Denmark. *Osteoporosis International.* 2005;16(2):134-141.

16. Cornell C. Internal fracture fixation in patients with osteoporosis. *Journal of the American Academy of Orthopaedic Surgeons.* 2003;11(2):109.

17. Schatzker J, Tile M. The AO (ASIF) method of fracture care. *Instr Course Lect.* 1980;29(41).

18. Kristiansen B, Christensen S. Plate fixation of proximal humeral fractures. *Acta Orthopaedica.* 1986;57(4):320-323.

19. Syed A, Agarwal M, Giannoudis P, Matthews S, Smith R. Distal femoral fractures: long-term outcome following stabilisation with the LISS. *Injury.* 2004;35(6):599-607.

20. Goh J, Shah K, Bose K. Biomechanical study on femoral neck fracture fixation in relation to bone mineral density. *Clinical Biomechanics.* 1995;10(6):304-308.

21. Stromsoe K, Kok W, Hoiseth A, Alho A. Holding power of the 4.5 mm AO/ASIF cortex screw in cortical bone in relation to bone mineral. *Injury.* 1993;24(10):656-659.
22. Hertel R, Jost B. Basic Internal Fixation in Osteoporotic Bone. In: An Y, ed. *Internal Fixation in Osteoporotic Bone*. New York: Thieme; 2002:108-115.
23. Giannoudis P, Schneider E. Principles of fixation of osteoporotic fractures. *The Journal of bone and joint surgery. British volume.* 2006;88(10):1272.
24. Nikolaou VS, Efstathopoulos N, Kontakis G, Kanakaris NK, Giannoudis PV. The influence of osteoporosis in femoral fracture healing time. *Injury.* 2009;40(6):663-668.
25. Kim WY, Han CH, Park JI, Kim JY. Failure of intertrochanteric fracture fixation with a dynamic hip screw in relation to pre-operative fracture stability and osteoporosis. *International orthopaedics.* 2001;25(6):360-362.
26. van Wunnik BP, Weijers PH, van Helden SH, Brink PR, Poeze M. Osteoporosis is not a risk factor for the development of nonunion: A cohort nested case-control study. *Injury.* Dec 2011;42(12):1491-1494.
27. Diamond TH, Clark WA, Kumar SV. Histomorphometric analysis of fracture healing cascade in acute osteoporotic vertebral body fractures. *Bone.* 2007;40(3):775-780.
28. Egermann M, Goldhahn J, Schneider E. Animal models for fracture treatment in osteoporosis. *Osteoporosis International.* 2005;16:129-138.
29. Turner S. How to Select your Animal Model for Osteoporosis Research. In: Duque G, Watanabe K, eds. *Osteoporosis Research: Animal Models*. London: Springer Verlag; 2011.
30. Nunamaker D. Experimental models of fracture repair. *Clinical orthopaedics and related research.* 1998;355:S56.
31. Holstein JH, Garcia P, Histing T, et al. Mouse Models for the Study of Fracture Healing and Bone Regeneration. In: Duque G, Watanabe K, eds. *Osteoporosis Research: Animal Models*. London: Springer Verlag; 2011.
32. Turner AS. Animal models of osteoporosis—necessity and limitations. *Eur Cell Mater.* 2001;1:66-81.
33. Wronski T, Cintron M, Doherty A, Dann L. Estrogen treatment prevents osteopenia and depresses bone turnover in ovariectomized rats. *Endocrinology.* 1988;123(2):681.
34. Wang J, Li W, Xu S, et al. Osteoporosis influences the middle and late periods of fracture healing in a rat osteoporotic model. *Chinese Journal of Traumatology.* 2005;8(2):111.
35. Kubo T, Shiga T, Hashimoto J, et al. Osteoporosis influences the late period of fracture healing in a rat model prepared by ovariectomy and low calcium diet. *The Journal of Steroid Biochemistry and Molecular Biology.* 1999;68(5-6):197-202.
36. Giro G, Sakakura CE, Gonçalves D, Pereira RMR, Marcantonio Jr E, Orrico SRP. Effect of 17β-Estradiol and Alendronate on the Removal Torque of Osseointegrated Titanium Implants in Ovariectomized Rats. *Journal of periodontology.* 2007;78(7):1316-1321.
37. Rocca M, Fini M, Giavaresi G, Nicoli Aldini N, Giardino R. Osteointegration of hydroxyapatite-coated and uncoated titanium screws in long-term ovariectomized sheep. *Biomaterials.* 2002;23(4):1017-1023.
38. Viera-Negrón YE, Ruan W, Winger JN, Hou X, Sharawy MM, Borke JL. Effect of ovariectomy and alendronate on implant osseointegration in rat maxillary bone. *Journal of Oral Implantology.* 2008;34(2):76-82.
39. Black D, Cummings S, Karpf D, et al. Randomised trial of effect of alendronate on risk of fracture in women with existing vertebral fractures. *The Lancet.* 1996;348(9041):1535-1541.

40. Rocca M, Fini M, Giavaresi G, Nicoli AN, Giardin R. Tibial implants: biomechanical and histomorphometric studies of hydroxyapatite-coated and uncoated stainless steel and titanium screws in long-term ovariectomized sheep. *The International journal of artificial organs.* 2001;24(9):649.

41. Wronski T, Dann L, Scott K, Cintron M. Long-term effects of ovariectomy and aging on the rat skeleton. *Calcified tissue international.* 1989;45(6):360-366.

42. Miller S, Wronski T. Long term osteopenic changes in cancellous bone structure in ovariectomized rats. *The Anatomical Record.* 1993;236(3):433-441.

43. Shen V, Dempster D, Birchman R, et al. Lack of changes in histomorphometric, bone mass and biochemical parameters in ovariohysterectomized dogs. *Bone.* 1992;13(4):311-316.

44. Arens D, Sigrist I, Alini M, Schawalder P, Schneider E, Egermann M. Seasonal changes in bone metabolism in sheep. *The Veterinary Journal.* 2007;174(3):585-591.

45. Li W, Duque G. Animal Models of Premature Aging. In: Duque G, Watanabe K, eds. *Osteoporosis Research: Animal Models*. London: Springer Verlag; 2011.

46. Hak DJ, Makino T, Niikura T, Hazelwood SJ, Curtiss S, Reddi AH. Recombinant human BMP-7 effectively prevents non-union in both young and old rats. *Journal of Orthopaedic Research.* 2006;24(1):11-20.

47. Meyer Jr RA, Tsahakis PJ, Martin DF, Banks DM, Harrow ME, Kiebzak GM. Age and ovariectomy impair both the normalization of mechanical properties and the accretion of mineral by the fracture callus in rats. *Journal of Orthopaedic Research.* 2001;19(3):428-435.

48. Ferguson VL, Ayers RA, Bateman TA, Simske SJ. Bone development and age-related bone loss in male C57BL/6J mice. *Bone.* 2003;33(3):387-398.

49. Glatt V, Canalis E, Stadmeyer L, Bouxsein ML. Age-Related Changes in Trabecular Architecture Differ in Female and Male C57BL/6J Mice. *Journal of bone and mineral research.* 2007;22(8):1197-1207.

50. Naik AA, Xie C, Zuscik MJ, et al. Reduced COX-2 Expression in Aged Mice Is Associated With Impaired Fracture Healing. *Journal of bone and mineral research.* 2009;24(2):251-264.

51. Chikazu D, Tomizuka K, Ogasawara T, et al. Cyclooxygenase-2 activity is essential for the osseointegration of dental implants. *International journal of oral and maxillofacial surgery.* 2007;36(5):441-446.

52. Watanabe K. Classical Models of Senile Osteoporosis. In: Duque G, Watanabe K, eds. *Osteoporosis Research: Animal Models*. London: Springer Verlag; 2011.

53. Jilka RL, Weinstein RS, Takahashi K, Parfitt AM, Manolagas SC. Linkage of decreased bone mass with impaired osteoblastogenesis in a murine model of accelerated senescence. *Journal of Clinical Investigation.* 1996;97(7):1732.

54. Egermann M, Ito K, Hofstetter W, Richards P. Fracture healing in a mouse model for senile osteoporosis2009.

55. Beppu K, Kido H, Watazu A, Teraoka K, Matsuura M. Peri-Implant Bone Density in Senile Osteoporosis-Changes from Implant Placement to Osseointegration. *Clinical Implant Dentistry and Related Research.* 2011.

56. Lin Z, Rios HF, Volk SL, Sugai JV, Jin Q, Giannobile WV. Gene Expression Dynamics During Bone Healing and Osseointegration. *Journal of periodontology.* 2011;82(7):1007-1017.

57. Ogawa T, Nishimura I. Genes differentially expressed in titanium implant healing. *Journal of dental research.* 2006;85(6):566-570.

58. Ornitz DM, Itoh N. Fibroblast growth factors. *Genome Biol.* 2001;2(3):3005.3001-3005.3012.

59. Zhang X, Ibrahimi OA, Olsen SK, Umemori H, Mohammadi M, Ornitz DM. Receptor specificity of the fibroblast growth factor family. *Journal of Biological Chemistry.* 2006;281(23):15694.

60. Funato N, Ohtani K, Ohyama K, Kuroda T, Nakamura M. Common regulation of growth arrest and differentiation of osteoblasts by helix-loop-helix factors. *Mol Cell Biol.* Nov 2001;21(21):7416-7428.

61. Rundle CH, Miyakoshi N, Ramirez E, Wergedal JE, Lau KHW, Baylink DJ. Expression of the fibroblast growth factor receptor genes in fracture repair. *Clinical orthopaedics and related research.* 2002;403:253.

62. Schmid GJ, Kobayashi C, Sandell LJ, Ornitz DM. Fibroblast growth factor expression during skeletal fracture healing in mice. *Developmental Dynamics.* 2009;238(3):766-774.

63. Colvin J, Bohne B, Harding G, McEwen D, Ornitz D. Skeletal overgrowth and deafness in mice lacking fibroblast growth factor receptor 3. *Nature Genetics.* 1996;12(4):390-397.

64. Deng C, Wynshaw-Boris A, Zhou F, Kuo A, Leder P. Fibroblast growth factor receptor 3 is a negative regulator of bone growth. *Cell.* 1996;84(6):911-921.

65. Valverde-Franco G, Liu H, Davidson D, et al. Defective bone mineralization and osteopenia in young adult FGFR3-/-mice. *Human molecular genetics.* 2004;13(3):271.

66. Valverde-Franco G, Binette J, Li W, et al. Defects in articular cartilage metabolism and early arthritis in fibroblast growth factor receptor 3 deficient mice. *Human molecular genetics.* 2006;15(11):1783.

67. Eswarakumar V, Schlessinger J. Skeletal overgrowth is mediated by deficiency in a specific isoform of fibroblast growth factor receptor 3. *Proceedings of the National Academy of Sciences.* 2007;104(10):3937.

68. Davidson D, Blanc A, Filion D, et al. Fibroblast growth factor (FGF) 18 signals through FGF receptor 3 to promote chondrogenesis. *Journal of Biological Chemistry.* 2005;280(21):20509.

69. Liu Z, Xu J, Colvin JS, Ornitz DM. Coordination of chondrogenesis and osteogenesis by fibroblast growth factor 18. *Genes Dev.* Apr 1 2002;16(7):859-869.

70. Liu Z, Lavine KJ, Hung IH, Ornitz DM. FGF18 is required for early chondrocyte proliferation, hypertrophy and vascular invasion of the growth plate. *Dev Biol.* Feb 1 2007;302(1):80-91.

71. Hung IH, Yu K, Lavine KJ, Ornitz DM. FGF9 regulates early hypertrophic chondrocyte differentiation and skeletal vascularization in the developing stylopod. *Dev Biol.* Jul 15 2007;307(2):300-313.

72. Jacob AL, Smith C, Partanen J, Ornitz DM. Fibroblast growth factor receptor 1 signaling in the osteo-chondrogenic cell lineage regulates sequential steps of osteoblast maturation. *Dev Biol.* Aug 15 2006;296(2):315-328.

73. Yu K, Xu J, Liu Z, et al. Conditional inactivation of FGF receptor 2 reveals an essential role for FGF signaling in the regulation of osteoblast function and bone growth. *Development.* Jul 2003;130(13):3063-3074.

74. Eswarakumar VP, Monsonego-Ornan E, Pines M, Antonopoulou I, Morriss-Kay GM, Lonai P. The IIIc alternative of Fgfr2 is a positive regulator of bone formation. *Development.* Aug 2002;129(16):3783-3793.

75. Kasemo B. Biocompatibility of titanium implants: surface science aspects. *The Journal of prosthetic dentistry.* 1983;49(6):832.

76. Hacking S, Zuraw M, Harvey E, Tanzer M, Krygier J, Bobyn J. A physical vapor deposition method for controlled evaluation of biological response to biomaterial chemistry and topography. *Journal of Biomedical Materials Research Part A.* 2007;82(1):179-187.

77. Sosale G, Hacking S, Vengallatore S. Topography analysis of grit-blasted and grit-blasted-acid-etched titanium implant surfaces using multi-scale measurements and multi-parameter statistics. *Journal of Materials Research.* 2008;23(10).

78. Hermida J, Bergula A, Dimaano F, Hawkins M, Colwell Jr C, D'Lima D. An in vivo evaluation of bone response to three implant surfaces using a rabbit intramedullary rod model. *Journal of Orthopaedic Surgery and Research.* 2010;5(1):57.

79. Hildebrand T, Rüegsegger P. Quantification of bone microarchitecture with the structure model index. *Computer Methods in Biomechanics and Biomedical Engineering.* 1997;1(1):15-23.

80. Hahn M, Vogel M, Pompesius-Kempa M, Delling G. Trabecular bone pattern factor--a new parameter for simple quantification of bone microarchitecture. *Bone.* 1992;13(4):327-330.

81. Teo J, Si-Hoe KM, Keh JEL, Teoh SH. Relationship between CT intensity, micro-architecture and mechanical properties of porcine vertebral cancellous bone. *Clinical biomechanics.* 2006;21(3):235-244.

82. Richard S, Torabi N, Franco G, et al. Ablation of the Sam68 RNA binding protein protects mice from age-related bone loss. *PLoS Genet.* 2005;1(6):e74.

83. Bauer TW, Schils J. The pathology of total joint arthroplasty. *Skeletal radiology.* 1999;28(9):483-497.

84. Wu P, Grainger DW. Drug/device combinations for local drug therapies and infection prophylaxis. *Biomaterials.* 2006;27(11):2450-2467.

85. Keselowsky BG, Bridges AW, Burns KL, et al. Role of plasma fibronectin in the foreign body response to biomaterials. *Biomaterials.* 2007;28(25):3626.

86. Henderson JE, Naski MC, Aarts MM, et al. Expression of FGFR3 with the G380R achondroplasia mutation inhibits proliferation and maturation of CFK2 chondrocytic cells. *Journal of bone and mineral research.* 2000;15(1):155-165.

87. Naski M, Wang Q, Xu J, Ornitz D. Graded activation of fibroblast growth factor receptor 3 by mutations causing achondroplasia and thanatophoric dysplasia. *Nature Genetics.* 1996;13(2):233-237.

88. Odgaard A, Gundersen H. Quantification of connectivity in cancellous bone, with special emphasis on 3-D reconstructions. *Bone.* 1993;14(2):173-182.

89. Odgaard A. Three-dimensional methods for quantification of cancellous bone architecture. *Bone.* 1997;20(4):315-328.

90. Xiao L, Naganawa T, Obugunde E, et al. Stat1 controls postnatal bone formation by regulating fibroblast growth factor signaling in osteoblasts. *Journal of Biological Chemistry.* 2004;279(26):27743.

91. Rundle C, Miyakoshi N, Ramirez E, Wergedal J, Lau K, Baylink D. Expression of the fibroblast growth factor receptor genes in fracture repair. *Clinical orthopaedics and related research.* 2002(403):253.

92. Schmid G, Kobayashi C, Sandell L, Ornitz D. Fibroblast growth factor expression during skeletal fracture healing in mice. *Developmental Dynamics.* 2009;238(3):766-774.

93. Haque T, Amako M, Nakada S, Lauzier D, Hamdy R. An immunohistochemical analysis of the temporal and spatial expression of growth factors FGF 1, 2 and 18, IGF 1 and 2, and

TGFbeta1 during distraction osteogenesis. *Histology and histopathology.* 2007;22(2):119.

94. Ellsworth J, Berry J, Bukowski T, et al. Fibroblast growth factor-18 is a trophic factor for mature chondrocytes and their progenitors. *Osteoarthritis and cartilage.* 2002;10(4):308-320.

95. Olsen S, Li J, Bromleigh C, et al. Structural basis by which alternative splicing modulates the organizer activity of FGF8 in the brain. *Genes & development.* 2006;20(2):185.

96. Zhang X, Ibrahimi O, Olsen S, Umemori H, Mohammadi M, Ornitz D. Receptor specificity of the fibroblast growth factor family. *Journal of Biological Chemistry.* 2006;281(23):15694.

97. Somia N, Verma IM. Gene therapy: trials and tribulations. *Nature Reviews Genetics.* 2000;1(2):91-99.

98. Thibault M, Nimesh S, Lavertu M, Buschmann MD. Intracellular Trafficking and Decondensation Kinetics of Chitosan–pDNA Polyplexes. *Molecular Therapy.* 2010;18(10):1787-1795.

99. Hendrikx PJ, Vermeulen J, Hagenbeek A, Vermey M, Martens A. LacZ staining in paraffin-embedded tissue sections. *Journal of Histochemistry & Cytochemistry.* 1996;44(11):1323.

APPENDIX

Animal Use Protocol for Mouse Research (begins on next page)

www.mcgill.ca/researchoffice/compliance/animal/forms

McGill University Animal Care Committee
RENEWAL of Animal Use Protocol

For: Research ☒ Teaching ☐ project

For Office Use Only:
Protocol #:
Approval end date:
Facility Committee:
Renewal#: 1st 2nd

Principal Investigator: Janet E HENDERSON **Protocol #** 5743

Protocol Title: MOLECULAR CONTROL of SKELETAL REGENERATION and REPAIR **Category:** D

Unit, Dept. & Address: JTN WONG Labs, 740 Ave Dr Penfield, Room 2300, Montreal H3A 1A4

Email: janet.henderson@mcgill.ca **Phone:** 514-934-1934-43358 **Fax:** NO FAX AVAILABLE

Funding source: CIHR

Start of Funding: April 2007 **End of Funding:** March 2012

Emergency contact #1 + work AND home phone #s: Janet E HENDERSON W: 514-934-1934-43358; H: 514-457-8849

Emergency contact #2 + work AND home phone #s: Huifen WANG W: 514-398-4400-094322; H 450-923-8013

1. Personnel and Qualifications

List the names of the Principal Investigator and of all individuals who will be in contact with animals in this study and their employment classification (investigator, technician, research assistant, undergraduate/ graduate student, fellow). Indicate if the Principal Investigator is not handling animals. If an undergraduate student is involved, the role of the student and the supervision received must be described. Training is mandatory for all personnel listed here. Refer to *www.animalcare.mcgill.ca* for details. Each person listed in this section must sign. ***(Space will expand as needed)***

Name	Classification	Animal Related Training Information		Species Handled	Signature *"Has read the original full protocol"*
		UACC on-line Theory course	Workshops + others		
HENDERSON, Janet E	PI	YES	will not handle animals		
HARVEY, Edward J	PI	YES	will not handle animals		
WANG, Huifen	Res Assist	YES	mouse/rat/WHMIS	mouse/rat	
CARLI, Alberto	MSc cand	YES	mouse/rat/WHMIS	mouse/rat	
GAO, Chan	PhD cand	YES	mouse/rat/WHMIS	mouse/rat	

Occupational Health Program information: *www.mcgill.ca/researchoffice/compliance/animal/occupational*

Approved by:

2. Approval Signatures

I will ensure that all collaborators and staff are aware of all changes to this protocol **Principal Investigator/ Course Director**		**Date:**
Chair, Facility Animal Care Committee		**Date:**
Animal Compliance Office		**Date:**
Chairperson, Ethics Subcommittee *(D level or Teaching Protocols Only)*		**Date:**
Approved Animal Use Period	**Start:**	**End:**

3. Summary (in language that will be understood by members of the general public)

AIMS AND BENEFITS: Describe, in a short paragraph, the overall aim of the study and its potential benefit to human/animal health or to the advancement of scientific knowledge *(was section 5a in main protocol).*

OBJECTIVE: To validate mesenchymal stem cell (MSC) seeded scaffolds and novel bone growth factors as potential therapeutic options to augment new bone formation in mouse and rat models of fracture healing.

APPROACH: Mice with targeted mutations in the genes encoding some growth factors and their receptors that are key modulators of bone development exhibit a reduction in their capacity to repair a surgically induced window defect in the thigh bone (femur) at four months of age. A variety of biocompatible materials seeded with MSC and carrying growth factors know to stimulate bone formation will be tested for their capacity to expedite bone healing in this simple mouse model. The biomaterials and biologics will also be tested for their capacity to prevent nonunion of a large osteotomy in the rat femur fixed internally with plate and screws to model surgical reconstruction of human bones after high impact trauma or removal of bone tumors.

BENEFITS: The incidence of defective bone healing increases with age, in individuals who have sustained therapeutic interventions that kill MSC and in "critical size" defects that are to big to heal in the absence of synthetic or devitalised bone grafts, which act as scaffolds but are poor inducers of new bone formation . Delayed fracture healing, nonunion and graft failure are predicted to increase dramatically over the next few decades along with the mean age of the global population. Bone tissue engineering with MSC, natural and synthetic scaffolds and osteogenic biologic agents is under intense investigation to promote new bone formation in patients with poor bone quality and critical size defects.

4. **Has there been any animal care issues?**	**YES** ☐ **NO** ☒ **if yes, supply details:**

5. If creating genetically modified animals or new combinations of genetic modifications, complete and attach a *Phenotype Disclosure form.*

If mice expressing new phenotype have been produced, submit a *Phenotype Disclosure form.*

Blank forms at *http://www.mcgill.ca/researchoffice/compliance/animal/forms/*

6. Procedures

a) For B and C level of invasiveness,

The procedures are the same as the original protocol: **YES** ☐ **NO** ☐

IF NO, complete the following:

Detail new procedures that are different from section 10a of the original protocol, including amendments *(include a copy of the entire revised procedure section 10a of the original protocol with the changes and/or new procedures in CAPS):*

b) For D level of invasiveness,

Include here <u>ALL</u> procedures described in the original protocol. New and changed procedures in CAPS *(was section 10a in main protocol); Please only attach SOPs related to new and changed procedures to this renewal form.*

SUMMARY of SOPs

SOP McGill 101.01 RECEIVING/ACCLIMATISATION
SOP McGill 101.02 RODENT ANALGESIA
SOP McGill 111.02 RAT ANESTHESIA
SOP McGill 110.03 MOUSE ANESTHESIA
SOP McGill 201.02 RODENT SURVIVAL SURGERY
SOP McGill 301.01 RODENT EUTHANASIA

SUMMARY of PROCEDURES

RECEIVING and ACCLIMATISATION
MICE ARE BRED IN HOUSE AND ARE THEREFORE ACCLIMATISED. RATS ARE ACCLIMATISED FOR 7 DAYS BEFORE BEING SUBJECTED TO SURGICAL PROCEDURES

SURVIVAL SURGERY on MICE and RATS

Survival surgery will be performed inside the barrier facility in the Procedure Room as per SOP McGill 201.02. Inhalation anesthesia will be induced as per SOP McGill 110.03 for mice and SOP McGill 111.02 for rats and a local anesthetic (lidocaine) applied prior to skin incision for all surgical procedures. All instruments, drapes and gauze will be steam sterilized and all surfaces and gloves wiped with Clidox and 70% ethanol prior to surgery. ANALGESIA: 0.1 MG/KG BUPRENORPHINE AND 5 MG/KG CARPROFEN IS ADMINISTERED 30 MINS PRIOR TO SURGICAL INTERVENTION. After shaving, the surgical site and surrounding area will be swabbed with 2% CHLORHEXIDINE and eye ointment administered. As per SOP McGill 101.02 animals will receive a SECOND AND THIRD DOSE OF BUPRENORPHINE IN THE 24 HOURS post-surgery. CARPROFEN IS ADMINISTERED 3 TIMES A DAY for 2 days POST SURGERY. Animals are expected to return to weight bearing within 24-48 hr and will have easy access to food placed on the bottom of the cage. All mice and rats will be allowed free ambulation and free access to food and water for up to six weeks post op when they will be euthanised as per SOP McGill 301.01 for tissue harvest.

MOUSE FEMORAL WINDOW DEFECT: DURATION 60 MINS After induction of anesthesia and analgesia a linear 3 mm incision will be made through the skin of the upper leg and the soft tissue teased apart to expose the femoral diaphysis. A hole will be pierced with a 22 guage needle through the cortical bone into the marrow cavity at the mid-diaphysis. Using a 1 mm dental burr and a drill rig to control the depth of incision, a window defect measuring 3 mm x 1 mm will be drilled on either side of the needle hole. Sterile MSC seeded scaffolds and test agents will be carefully placed in the RIGHT femoral defect and the control LEFT will receive an acellular scaffold before the overlying soft tissue and skin are re-apposed and sutured.

RAT FEMORAL CRITICAL SIZE DEFECT: DURATION 90 MINS After induction of anesthesia and analgesia a linear incision will be made through the skin of the RIGHT femur and the soft tissue teased apart to expose the entire femoral diaphysis. A custom polyethylene plate will be aligned to span the mid femoral diaphysis and attached to the bone using threaded screws (RatFix). A segment of bone measuring 5 mm will then be removed using an oscillating saw with copious irrigation to prevent thermal damage.

Bone chips will be removed using gentle lavage with sterile PBS. Sterile MSC seeded scaffolds and test agents will be carefully positioned in the defect before the overlying soft tissue and skin are re-apposed and sutured.

7. Endpoints

a) For B and C level of invasiveness,

The procedures are the same as the original protocol: YES ☐ NO ☐

IF NO, supply new endpoints that are different from the original protocol:

Experimental endpoints:

Clinical endpoints:

b) For D level of invasiveness,

Include here ALL endpoints, including the ones described in the original protocol as well as new and changed endpoints in CAPS:

Experimental endpoints:
All donor animals will be euthanised by exsanguination under anesthesia to harvest bone marrow for ex vivo culture and seeding into variuos scaffold materials. Surgically modified mice (window defect) will be euthanised as per SOP McGill 301.01 by exsanguination under anesthesia two or four weeks post op, and rats (segmental defect) up to 12 weeks post op. Bone regeneration and fracture repair will be assessed using micro CT imaging, histological and molecular analyses.

Clinical endpoints:
ANIMALS WITH 20% WEIGHT LOSS AND BODY CONDITION SCORE LESS THAN 2 WILL BE EUTHANISED
All animals will be monitored twice a day for the first two days following an intervention and once a day thereafter for the duration of the experiment. Signs of distress, including loss of appetite, lethargy, weight loss, pilo-erection, swelling around surgical wounds or failure to resume weight bearing after 3 days will be noted and the animals euthanised if warranted.. Animals will be weighed every day for 5 days post op then twice a week thereafter.

8. Hazards (check here if none are used: ☐)

a) Are the hazards different from original protocol? (infectious, radioactive, toxic, carcinogen, tumours)

YES ☐ NO ☒ if yes, supply details (material, risks, precautions):

b) Have the cell lines been tested for human and animal pathogens? YES:☐ NO:☐ None used:☒

9. Description of Animals to be used in the coming year (only):

Quality Control Assurance: To prevent introduction of infectious diseases into animal facilities, a health status report or veterinary inspection certificate may be required prior to receiving animals from all non-commercial sources or from commercial sources whose animal health status is unknown or questionable. Quarantine and further testing may be required for these animals. *If more than 6 columns are needed, please attach another page*

	Sp/strain 1	Sp/strain 2	Sp/strain 3	Sp/strain 4	Sp/strain 5	Sp/strain 6
Species	RAT	MOUSE	MOUSE	MOUSE	MOUSE	
Supplier/Source	Charles River	Charles River	Henderson	Charles River	Henderson	
Strain	S Dawley	C3H	C3H FGFR3 mutant	C57Bl6	C57Bl6 PTHrP mutant	
Sex	M/F	F	M/F	F	M/F	
Age/Wt	4 mo/350g	2 mo/ 30g	4 mo/30g	2 mo/30g	4 mo/30g	
# To be procured	216	24	0	24	0	
# Produced by in-house breeding	0	0	162	0	162	
# Other (e.g.field studies)	0	0	0	0	0	
TOTAL# /YEAR	**216**	**24**	**162**	**24**	**162**	

10. Explanation of Animal Numbers:

BASED ON THE EXPERIMENTAL OBJECTIVES OF THE PROJECT, describe the number of animals required for one year. Include information on experimental and control groups, # per group, and failure rates.

For breeding, specify how many adults are used, number of offspring produced, and how many offspring are used in experimental procedures. The arithmetic explaining how the total of animals for each column in the table above is calculated should be made clear.

BREEDING STOCK: All mice to be used in these studies will be obtained from the Henderson breeding colonies, which are maintained by a full time animal care technician with 9y experience. Mice are used as they become available and rats will be purchased from Charles River. The number of breeding cages varies over time depending on the availability of HQP to perform the surgery. On average 2-4 cages of backcross animals are maintained to generate heterozygous offspring for 3 different mutations. Up to 8 cages of 1 male with 4 female heterozygotes is maintained to generate the experimental offspring.

EXPERIMENTAL ANIMALS: From previous work we have established a 1:1 donor to recipient ratio for mouse MSC transplantation studies and anticipate that 1:3 ratio will be required for the rat studies. We propose to perform three independent experiments with 6 recipient animals in each. These numbers account for any losses that might occur during MSC processing or during surgery in recipient animals. Loss of mice as a result of surgical intervention is less than 10% and power analysis predicts that 10 mice/group will be required for statistical significance. The critical size defect in the rat is more challenging and can have up to 30% failure rate.

COLUMN 1: Total 216 M/F SPRAGUE DAWLEY rats to be purchased from Charles River
8 rats/condition x 9 conditions x 3 end points

COLUMN 2: Total 24 C3H F WT mice to be purchased from Charles River
Backcross with M FGFR3+/- to generate FGFR3+/- mice for intercross

COLUMN 3 Total 162 C3H M/F FGFR3+/+ and -/- to be generated from FGFR3+/- intercross
6 mice/condition x 6 conditions x 2 genotypes (+/- mice are used for intercross)

COLUMN 4 Total 24 C57Bl6 F WT mice to be purchased from Charles River
Backcross with M PTHrP+/- to generate PTHrP+/- for intercross

COLUMN 5 Total 162 C57Bl6 M/F PTHrP+/+ and +/- to be generated from PTHrP+/- intercross
6 mice/condition x 6 conditions x 2 genotype (-/- mice are neonatal lethal)

Specify numbers for breeders that are procured and/or produced in-house and ensure that these numbers are included in the table of section 9 above:
see above

Submit to your local Facility Animal Care Committee. Please note that after two renewals, a full protocol needs to be submitted.

This approval does not imply that space will be made available. If a major increase of space needs is anticipated, please contact the appropriate animal facility manager.